Chemical Geology 550 (2020) 119743

Contents lists available at ScienceDirect

Chemical Geology

journal homepage: www.elsevier.com/locate/chemgeo

Towards a global quantification of volcanogenic aluminosilicate alteration rates through the mass balance of strontium in marine sediments

W.-L. Hong[a,*], M.E. Torres[b], S. Kutterolf[c]

[a] Geological Survey of Norway (NGU), Trondheim, Norway
[b] College of Earth, Ocean and Atmospheric Sciences (CEOAS), Oregon State University, Corvallis, OR, USA
[c] GEOMAR Helmholtz Centre for Ocean Research, Kiel, Germany

ARTICLE INFO

Editor: Karen Johannesson

Keywords:
Volcanogenic aluminosilicate
Strontium
Numerical modeling

ABSTRACT

Despite the important role that volcanogenic aluminosilicate (VA) alteration has on elemental cycles in marine sediments, there is no mechanism to arrive at a global assessment of this process. To quantify the VA alteration rates from Japan, New Zealand (NZ), and Costa Rica, we develop a mass balance approach that is constrained by the strontium concentrations and $^{87}Sr/^{86}Sr$ ratios in pore fluids, authigenic carbonates, and VAs. We derive VA alteration rates ranging from 10^1 to 10^3 nmole Sr/m^3 bulk sediment/yr with the highest rate obtained for Tuaheni, NZ (Site GeoB20802), which has the youngest sediment. We show that $^{87}Sr/^{86}Sr$ ratios of VA derived from this mass balance approach are significantly higher than the reported ratios from volcanic glass samples, indicating a concomitant role of feldspar dissolution and/or authigenic clay formation. Most of the strontium released during VA alteration is precipitated as authigenic carbonates, with important implications for carbon inventories. The VA alteration rates derived from this approach can also be used to quantify the release of other critical elements, such as iron that can stimulate formation of Fe-carbonates and/or fuel microbial activity at depth.

1. Introduction

Volcanogenic aluminosilicates (VAs) are defined as materials erupted from volcanoes and include volcanic glass as well as crystalline silicates such as plagioclase, biotite, pyroxene, and amphibole (Sutton et al., 1995; Yokoyama and Banfield, 2002; Wilson et al., 2006). VA is easily recognized as tephra layers (e.g., Kutterolf et al., 2008a) but also occurs as disseminated fine grain materials within marine sediment, as documented by Scudder et al. (2009, 2016). Alteration of VA releases bicarbonate, nutrients (e.g., silica and iron) and cations (e.g., calcium and iron) with significant consequences for the global element budgets (Lawrence et al., 1979; Gieskes and Lawrence, 1981; Plank and Langmuir, 1998; Wallmann et al., 2008; Torres et al., 2020). Because of their widespread distribution and highly reactive nature, VA alteration drives many diagenetic processes in hemipelagic sediment sections (Kastner, 1981; Wallmann et al., 2008; Longman et al., 2019; Torres et al., 2020). For example, the iron, manganese, and aluminum released during VA alteration are thought to enhance the preservation of organic carbon through complexation (Mayer, 1994; Basile-Doelsch et al., 2007; Homoky et al., 2011; Roy et al., 2013; Barber et al., 2017; Longman et al., 2019). More recently, iron released from VA has been shown to fuel microbial activity (e.g., Fisk et al., 1998; Henri et al., 2016; Luo et al., 2020). Cations released from VA alteration also drive authigenic carbonate precipitation, which plays a significant role in the global carbon cycle (Sample et al., 2017; Phillips et al., 2018; Torres et al., 2020). The silica released to the pore fluid drives the formation of amorphous silica and authigenic clay minerals (Jeans et al., 2000; Mork et al., 2001; White et al., 2011; Spinelli and Hutton, 2013). Diagenetic carbonate and silicate minerals significantly impact the geomechanical and hydrogeologic properties of the sediment column, with potential consequences for the permeability evolution of a formation (Spinelli et al., 2007; White et al., 2011; Rose et al., 2014). Consequently, there is a growing need for a mechanism to quantify VA alteration rates on local and global scales.

For the past decades, great efforts have been made to quantify the dissolution of volcanic glass in laboratory experiments to understand the factors that control its reaction kinetics (Table 1). Yokoyama and Banfield (2002) collected outcrop samples from Kozushima Island, Japan with different degrees of weathering. They estimated an alteration rate of 6×10^{-19} mol $Si/cm^2/s$ over the past 52,000 years. Additional laboratory experiments using the same set of samples yielded rates ranging from 10^{-18} to 10^{-16} mol $Si/cm^2/s$, depending on the

* Corresponding author at: Department of Geological Sciences, Stockholm University, Sweden.
E-mail address: wei-li.hong@geo.su.se (W.-L. Hong).

https://doi.org/10.1016/j.chemgeo.2020.119743
Received 16 October 2019; Received in revised form 4 June 2020; Accepted 9 June 2020
Available online 15 June 2020

Table 1
A summary of volcanic glass dissolution rates from the literature.

Location	Rate (10^{x})[‡]	Time scale	Method	Temperature	pH	Rock type	Ref	note
Kozushima Island (Japan)	−18.2	52,000 years	Field observations	20 °C	6–7	Rhyolite	YB	
	−16.3 to −17.3	100 days	Lab	20 °C	6–7	Rhyolite	YB	
	−15.5 to −17.1	277 days	Lab	20 °C	6–7	Rhyolite	Y	Time-dependent
Iceland and Long Valley (California, USA)	−11.2 to −13.9[*]	24 h	Lab	25–74 °C	~4 and 10.6	Rhyolite, dacite, basalt, mugearite	W	Far-from-equilibrium condition
Öraefajökull (Iceland)	−10.8 to −13.7	3–10 days	Lab	40–200 °C	2–10.1	Rhyolite	De	Steady-state rate, consistent with Arrhenius equation
Mt. Fuji (Japan)	−13.7 to −14.7	240–6000 years	Modeling of solution SiO_2	20 °C	~7	Basalt	Sh	Steady-state rate
N.A.	−11.3	190 days	Si and O isotope tracers	90 °C	~7–8	Artificial borosilicate glass	V	
N.A.	−15.7 to −16.1	1000 days	Lab	30 and 90 °C	~9–10	Artificial basaltic glass	P	
Mt. St. Helens (USA)	−17 to −18[†]	4 years	Field observations	4–5 °C	~4.5–7	Tephra	Da	
Rio Icacos (Puerto Rico) Panola (Georgia) Riverbank (Cali., USA)	−11.8 to −12.6[†]	0.2–0.4 Ma	Modeling of Si mass balance	16–22 °C	4.9–7.4	Granitoid	St	
Nicaragua	−15 to −17	Days to months	Lab	25–100 °C		Mafic and felsic glass	Sc	1, 200, and 400 bars applied
Juan de Fuca Ridge and Hess Depression	N.A.	149–460 days	Lab	70 and 150 °C	5.4–7.7	Basaltic glass and diabase	Se	500 bars applied

YB: Yokoyama and Banfield (2002); Y: Yokoyama (2013); W: Wolff-Boenisch et al. (2004); De: Declercq et al. (2013); Sh: Shikazono et al. (2005); V; Valle et al. (2010); P: Parruzot et al. (2015); Da: Dahlgren et al. (1999); St: Stonestrom et al. (1998); Sc: Schacht (2005); Seyfried Jr and Bischoff (1979). N.A.: not available.

[‡] Unit: mole Si/cm^2/s.

[*] Geometric surface area-normalized rates.

[†] Bulk sediment-normalized rates.

dissolved Si concentration, reaction time, and experiment setup (Yokoyama and Banfield, 2002; Yokoyama, 2013). Wolff-Boenisch et al. (2004) determined the dissolution rates of volcanic glass samples from Iceland and California (USA) that covered various glass compositions (rhyolite, dacite, basaltic, and mugearite). The experiments were conducted at different conditions pH (4 and 10.6) and temperature (25–74 °C) and showed that the dissolution rate is a function of the SiO_2 content in the volcanic glass. In a more recent work, Declercq et al. (2013) conducted experiments to determine the dissolution rate of rhyolite volcanic glass from Iceland under a wide range of pH (2–10.1) and temperature (40–200 °C) conditions. They showed that dissolution rate constants are consistent with predictions from the Arrhenius equation (Arrhenius, 1889) with additional dependencies on the activities of dissolved silica and hydrogen ions. Besides solution chemistry and temperature, Schacht (2005) showed that elevated pressure can also accelerate volcanic glass alteration and highlighted the importance of burial history on glass alteration.

These efforts show the complex kinetics of VA alteration and the dependence of VA alteration on the sediment environment as well as burial history, which make estimates of the in-situ reaction rates very challenging. Here we develop a numerical model that allows for determining in situ VA alteration rates in hemipelagic sediments that receive input from volcanogenic sources. The model is based on a mass balance of strontium (Sr) concentrations and $^{87}Sr/^{86}Sr$ isotopic ratios in pore fluids, authigenic carbonates and VAs. This strategy allows us to derive effective VA dissolution rates at four continental margin settings (Fig. 1) with sediment ages ranging from 110 ka to 29 Ma. Our model does not explicitly consider factors that are known to affect VA dissolution (such as surface area of VA, pH, etc.) but constrain the rate from a strontium mass balance point of view. Given the variability of VA composition, its physical characteristics and the diverse formation fluids encountered in nature, we argue that our approach is more likely to yield genuine estimates on VA turnover in marine sediment. Future applications of this model to a greater dataset will allow for a comprehensive assessment of VA alteration on a global scale.

We consider strontium as an adequate tracer for VA alteration due to the following reasons: 1) the strontium system in hemipelagic sediments is well-studied (e.g., Faure and Powell, 1972; Elderfield and Gieskes, 1982; Elderfield, 1986; Palmer and Edmond, 1989; Veizer, 1989; Joseph et al., 2012) and only affected by a hand-full of reactions; 2) $^{87}Sr/^{86}Sr$ ratios can be used to differentiate alteration of volcanic materials vs. continental-derived silicates (Veizer, 1989). The ratios are not affected by carbonate precipitation nor are they fractionated biologically (Veizer, 1989; Vollstaedt et al., 2014; Pearce et al., 2015); and 3) the analysis of strontium and its isotopic composition in geo-materials are well established with a rich collection of data already available in the literature for future global assessment efforts (e.g., Elderfield and Gieskes, 1982; Joseph et al., 2012; Kim et al., 2013; Joseph et al., 2013a; Joseph et al., 2013b; Solomon et al., 2014; Moen et al., 2015; Ross et al., 2015; Kim et al., 2016; Sample et al., 2017; Phillips et al., 2018). The data we use in this study were collected from sites characterized by significant VA input: Integrated Ocean Drilling Program (IODP) Exp. 322 Site C0012 (Nankai Trough, Japan) (Underwood et al., 2010; Expedition 333 Scientists, 2012; Sample et al., 2017); IODP Exp. 337 Site C0020 (Shimokita, Japan) (Expedition 337 Scientists, 2013a, Expedition 337 Scientists, 2013b, Moen et al., 2015, Phillips et al., 2018); IODP Exp. 344 Site U1413 (Costa Rica) (Harris et al., 2013a, Harris et al., 2013b, Ross et al., 2015), and R/V Sonne Exp. 247 Site GeoB20802 (Tuaheni, New Zealand) (Huhn, 2016; Luo et al., 2020) (Fig. 1). The strontium system in these locations reflects different end-member conditions (see site description for details) suitable for establishing our mass balance approach.

2. Geological background

We compiled data from three different subduction zones (Fig. 1) to

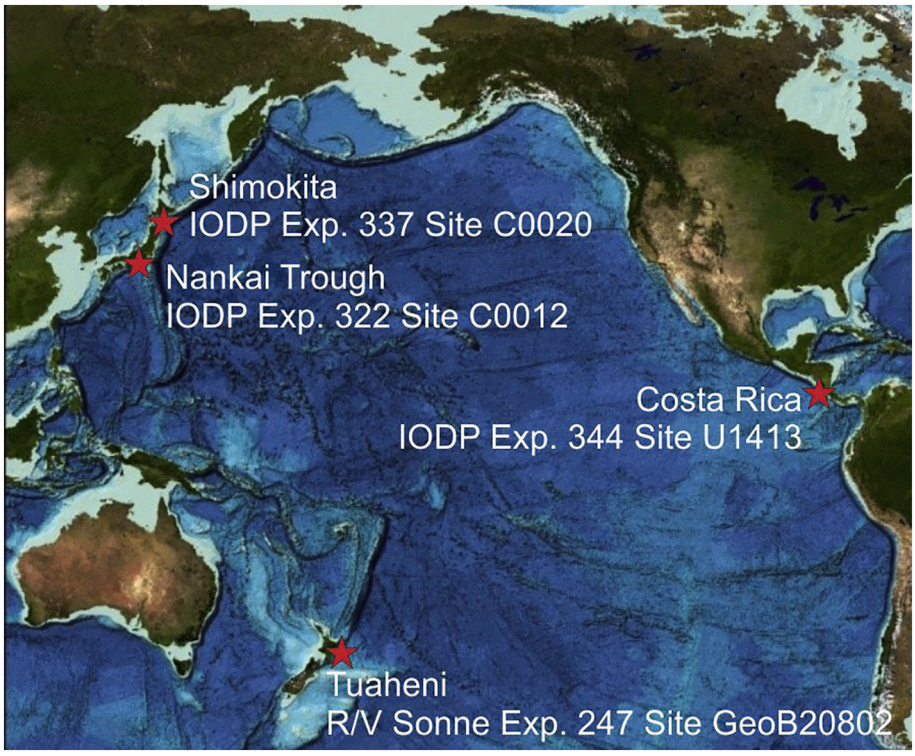

Fig. 1. The four locations investigated. Base map image reproduced from the GEBCO world map 2014, ww.gebco.net.

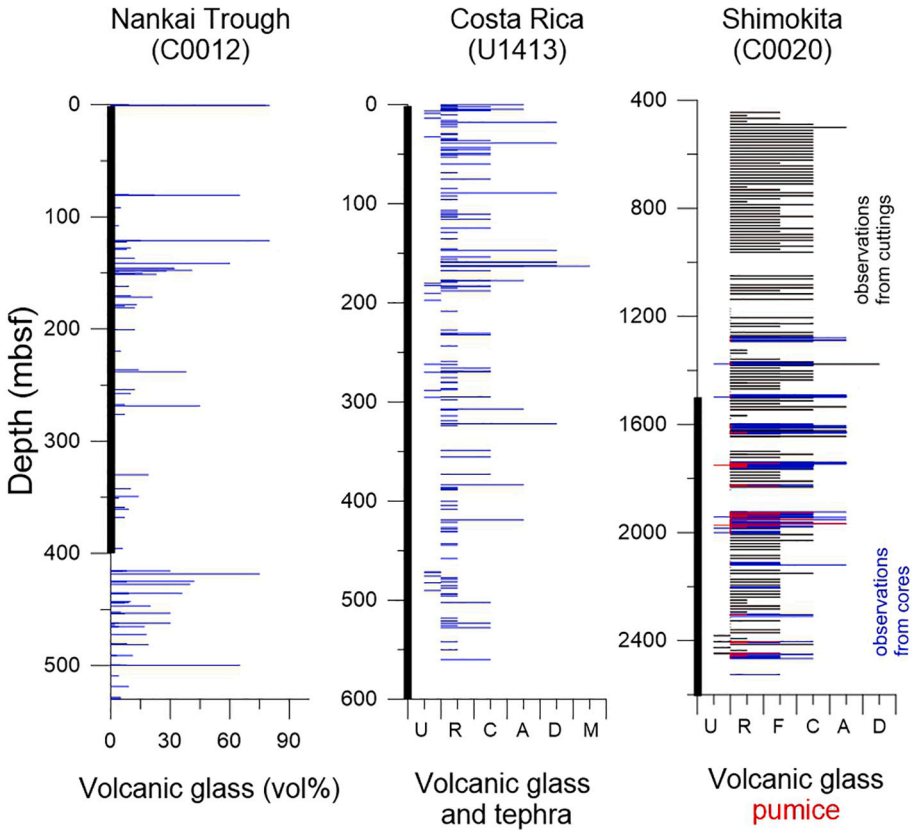

Fig. 2. Downcore distribution of volcanic materials from Sites C0012, U1413, and C0020 (Expedition 333 Scientists, 2012, Expedition 337 Scientists, 2013b, Harris et al., 2013b). Notice that for Site C0020, we included volcanic glass observations from both cuttings (black bars) and cored sediments (blue bars) with the latter only available from 1256 to 2466 mbsf. Observations of pumice (red bars) were also indicated. The black bar overlapping the y-axis for each site marks the depth range focused in our model. The following classification was used for Site U1413: R = rare (< 1 vol%), C = common (1–10 vol %), A = abundant (10–50 vol%), D = dominant (50–80 vol%), M = major (> 80 vol%). The following classification was used for Site C0020: U = unavailable, R = rare (< 0.1 vol%), F = few (0.1–1 vol%), C = common (1–10 vol%), A = abundant (10–50 vol%), D = dominant (> 50 vol%). (For interpretation of the references to color in this figure legend, the reader is referred to the web version of this article.)

generate a comprehensive view of VA alteration along convergent margins. We include examples from both accretionary (e.g., Nankai Trough and Tuaheni) and erosive (e.g., Costa Rica) margins, defined by the material source to the down-going slab. In erosive margins net removal of upper plate material occurs at the front or at the base of the forearc, whereas accretionary margins accumulate the sediment from the incoming plate at the front of the forearc or by underplating, leading to a net growth of the margin (von Huene and Scholl, 1991;

Clift and Vannucchi, 2004). The sediment from Site GeoB20802 was recovered from the shelf region thought to represent the source material in the Tuaheni slide complex, and to contrast with sediments from the input section to the Nankai Trough system. The material sampled at Site GeoB20802 is not directly associated with the subducting processes at the Hikurangi margin, rather reflects a nearshore marine environment where ash alteration impacts biogeochemical cycling (Huhn, 2016).

2.1. Nankai Trough, IODP Exp. 322

Nankai Trough formed during the northwest subduction of Philippine Sea plate beneath the Euroasian plate. This seismically active area has been intensively drilled by ODP and IODP expeditions, in an effort to understand hydrologic processes and fault zone behavior during earthquake nucleation offshore Japan. During IODP Exp. 322 and 333, sediments and pore fluids were sampled at Sites C0011 and C0012 to fully characterize the Shikoku Basin section approaching and entering the Nankai Trough subduction zone (Underwood et al., 2003). In the simplest view, the Shikoku Basin strata can be grouped into two units (upper and lower Shikoku Basin facies), which are overlain by Quaternary turbidites of the Nankai trench wedge. At Site C0012 sediments consist of ash-bearing hemipelagic muds, a bioturbated mudstone interbedded with tuffaceous/volcaniclastic sandstone, siliciclastic turbidites and a basal volcaniclastic-rich facies (Saito et al., 2010; Henry et al., 2012). The relative ash content of the sediment sequences in the incoming plate reflects the regional and time-dependent volcanic activity of the surrounding arcs (Kennett et al., 1977; Ledbetter and Sparks, 1979; Cambray et al., 1993; Kutterolf et al., 2008b; Mahony et al., 2011) (Fig. 2). The number and thickness of ash layers decrease significantly below the Unit I/II boundary. However, estimates of disseminated ash based on geochemical proxies is thought to remain high (Scudder et al., 2009). The age of the sediments from Site C0012 was determined by shipboard biostratigraphers and is roughly 20 Ma at 530 meters below seafloor (mbsf) (Saito et al., 2010) (Table 2).

2.2. Tuaheni, New Zealand, MeBo driling SO247

The northern Hikurangi margin includes a flat, 20–30 km-wide continental shelf, a steep sediment-starved slope, and a 3500 m-deep subduction trough. Up to a kilometer of Quaternary sediment accumulates in ponded basins along the northern Hikurangi margin continental shelf (Lewis et al., 2004) and slope (Orpin, 2004; Orpin et al., 2006; Paquet et al., 2006). The upper 500–800 m of the upper continental slope was formed by a prograding low-stand accretion consisting of fine sandy up to clayey sediments bearing a multiplicity of volcanic ashes (Paquet et al., 2011). The presence of vitric ash components in sediments from the Poverty Bay margin have been attributed to its location downwind of the Taupo Volcanic Zone (e.g., Orpin, 2004; Gerber et al., 2010; Pouderoux et al., 2012). In places, tephra are thoroughly reworked by intense bioturbation (Huhn, 2016). Consistency in tephrostratigraphy data however indicates that despite slope instability, hemipelagic sedimentation in Poverty Bay ($\sim$0.06 cm year^{-1}) is the dominant background process operating at millennial time scales since the mid-Holocene (Orpin, 2004).

During the MeBo 200 drilling campaign in 2016, Site GeoB20802 was selected as a reference for the undisturbed slope section in the vicinity of the Tuaheni slide complex (Huhn, 2016). Drilled sediments consist mostly of greenish-grey clayey silts. Interbedded ash layers 1–2 cm in thickness were observed in the upper 20 mbsf (Huhn, 2016) occurring either as reworked ash or in coarse-grained turbidites. They are exclusively composed of volcaniclastic debris (glass shards and pumiceous lapilli mostly) as identified by their typical whitish-greyish color and high values of magnetic susceptibility ($>$40 SI) from admixed ferro-magnesia and opaque Fe-rich minerals. The age of the sediment from Site GeoB20802 was derived by using the sedimentation rate given in Luo et al. (2020), and is ca. 0.08 cm/yr.

2.3. Costa Rica subduction zone, IODP Exp. 344

The region targeted by the Costa Rica Seismogenesis Project (CRISP), offshore the Osa Peninsula, is part of an extensive erosional subduction zone that extends from Guatemala to Costa Rica (Ranero et al., 2000; Ranero and von Huene, 2000; Vannucchi et al., 2004). CRISP aims to understand the processes that control fault zone behavior during earthquake nucleation and rupture propagation at erosional subduction zones. This region is characterized by variable sediment supplies (Schindlbeck et al., 2016b), fast convergence rates, abundant seismicity, and changes in subducting plate relief along strike. Site U1413 was drilled in the middle slope region along a 3-D seismic line (Bangs et al., 2015). Three lithostratigraphic units were distinguished in the sediment section of Site U1413. The upper $\sim$150 m of sediments contain three mass transport deposits that are several meters in thickness (Harris et al., 2013a). Twelve distinct tephra layers back to 1.6 Ma were recovered at the top of the section and between 135 and 180 mbsf (Fig. 2) (Schindlbeck et al., 2016a).

2.4. Shimokita, Japan, IODP Exp. 337

Site C0020 is located off the Shimokita Peninsula, Japan, at a water depth of 1180 m in a forearc basin formed by the subduction of the Pacific plate under the Okhotsk plate. Cores were recovered only from

Table 2
Input parameters for the four investigated sites.

Variable	Unit	Nankai Trough C0012	Tuaheni GeoB20802	Costa Rica U1413	Shimokita C0020	Meth.[a]
(a) L	m	400	110	620	1000	
(b) T	Ma	20 ➔ 0	0.20 ➔ 0	1.6 ➔ 0	29 ➔ 20	a.m.
(c) dt	Ma	0.01	6.4E-5	2.6E-3	0.06	m
(d) dx	m	0.5	0.44	0.62	2	m
(e) v_{inf}	m/yr	1.5E-5	7E-4	3.83E-4	7E-5	a.m.
(f) ϕ_0		0.8	0.76	0.7	0.9	m, Eq. (4)
(g) $\phi_{f.\ inf}$		0.38	0.48	0.45	0.2	
(h) α		−0.005	−0.07	−0.008	−0.001	
(i) k_c	1/yr	4E-6	5E-5	7E-6	6E-9	m
(j) R_{carb1}		1.12	1.12	1.12	1.12	m
(k) R_{carb2}		0.85	0.8	0.9	0.9	m
(l) k_A	1/yr	1.4E-7	7E-6	1.6E-7	2E-7	m
(m) Sr in VA (or Γ_A)	ppm	400	400	400	400	m, Eq. (11)
(n) Sr/Ca in carbonates	mmol/mol	4.5	3.1	4.5	0.23	m

[a] Methods for the determination of the input parameters: "a.m."- age model (see *Geological Background* for details) and "m"- model iteration or see specific equations for explanations.

1256 to 2466 mbsf, with sediment ages spanning from 20 to 29 Ma (Phillips et al., 2016), with the main objective of gaining information on the relationship between deep coalbeds and microbial activity (Expedition 337 Scientists, 2013a, Kawai et al., 2014, Inagaki et al., 2015, Glombitza et al., 2016, Fang et al., 2017, Phillips et al., 2017, Trembath-Reichert et al., 2017). The site experienced a transition from terrestrial to marine depositional environments (Gross et al., 2015; Bowden et al., 2019) with high organic matter-rich sediments recovered from the terrigenous sediments (Expedition 337 Scientists, 2013b). A series of coal beds that are 0.3 to 7.3 m thick were recovered at depths between ~1500 to 2500 mbsf (Expedition 337 Scientists, 2013a). Pristine and altered volcanic glass was often observed from smear slides with its abundance varying from few (0.1–1 vol%) to common (1–10 vol%) (Fig. 2). The age of the sediments from Site C0020 was crudely established by Gross et al. (2015), as ranging between 20 and 29 Ma for the cored section (Table 2).

3. Modeling of Sr mass balance

3.1. Numerical model framework

We developed a transport-reaction model to quantify the production and consumption of strontium in marine sediments. The model has a fixed depth range of observation (row (a) in Table 2) with sediment and pore fluid being buried through the column. For Site C0020, we modeled only the 1000 m of sediments that correspond to the depths from 1500 to 2500 mbsf where sediment and pore fluid data are available. Seafloor is always at zero depth with constant properties except for changes in the $^{87}Sr/^{86}Sr$ and strontium concentration of coeval seawater (see later for details). Essentially, the model calculates the mass balance of strontium in each depth and time intervals defined for the investigated sites. Strontium is released to pore fluids from VA decomposition and consumed via carbonate precipitation. The conservation of strontium in a unit volume of bulk sediments is set as follow:

$$\frac{\partial(M_x^t)}{\partial t} = \frac{\partial F_x^t}{\partial x} + \Sigma R_x^t \tag{1}$$

M: mole or gram of strontium in pore fluid/carbonate/VA in bulk sediments as a function of depth and time;
F: volumetric flux of pore fluid, carbonate, or VA as a function of depth and time (mole or gram/m^2 bulk sediment/year);
R: sum of different reactions considered as a function of depth and time.
t and x: time and depth (meter and year).

For strontium in the solid phases (carbonate and VA), Eq. (1) is reformulated as follow:

$$\frac{\partial[\phi_{s.x} C_x^t]}{\partial t} = -\frac{\partial[v_{sed.x}\phi_{s.x} C_x^t]}{\partial x} + \Sigma R_{s.x}^t \tag{2}$$

$\phi_{s.\ x}$: dry sediment volume fraction as a function of depth;
$C_x{}^t$: gram of carbonate or VA ($A_x{}^t$:) in dry sediments as a function of depth and time;
$v_{sed.\ x}$: dry sediment burial velocity as a function of depth (m bulk sediment/yr);
$\Sigma R_{s.\ x}{}^t$: sum of reactions for the solid phases (gram carbonate or VA/m^3 bulk sediments/yr).

For dissolved strontium and calcium in the pore fluid, Eq. (1) becomes:

$$\frac{\partial(\phi_{f.x} S_x^t)}{\partial t} = \frac{\partial\left(D_x \frac{\partial(\phi_{f.x} S_x^t)}{\partial x} - (v_{f.x} + v_{ext.x})\phi_{f.x} S_x^t\right)}{\partial x} + \Sigma R_{f.x}^t \tag{3}$$

$\phi_{f.\ x}$: pore fluid volume fraction as a function of depth;
$S_x{}^t$: Sr or Ca concentration in solution as a function of depth and time (mole/m^3 pore space/year);
$v_{f.\ x}$: pore fluid burial velocity as a function of depth (m bulk sediment/yr);
$v_{ext.\ x}$: external fluid velocity as a function of depth (m bulk sediment/yr);
D_x: strontium diffusion coefficient as a function of depth (m^2 bulk sediment/yr);
$\Sigma R_{f.\ x}{}^t$: sum of reactions for the solute as a function of depth and time (mole Sr/m^3 bulk sediment/yr).

The volume partition between the solid and pore fluid phases is determined by the downcore porosity profile (Expedition 333 Scientists, 2012, Expedition 337 Scientists, 2013b, Harris et al., 2013b, Huhn, 2016), which is defined as:

$$\phi_{f.x} = \phi_{f.inf} + (\phi_0 - \phi_{inf})Exp(-\alpha x) \tag{4}$$

$\phi_{f.\ inf}$: porosity at an infinite depth where the minimum porosity is achieved (row (g) in Table 2);
ϕ_0: porosity at sediment-water interface (row (f) in Table 2);
α: decay constant for porosity (row (h) in Table 2).

Strontium can be transported through diffusion in the pore fluid and/or advection (in both pore fluid and sediments through burial) from and to the adjacent cells. We adopted the diffusion coefficient for strontium at 25 °C (Boudreau, 1997) and corrected it with tortuosity that was calculated from porosity:

$$D'_{Sr.x} = \frac{D_{Sr}^{sw}}{1 - Ln(\phi_{f.x}{}^2)} \tag{5}$$

$D_{Sr.\ x}'$: diffusion coefficient of strontium in bulk sediments;
$D_{Sr}{}^{sw}$: diffusion coefficient of strontium in seawater.

Sediment and pore fluid advection is due to burial and compaction of bulk sediment. We assumed porosity to be constant in time (i.e., steady-state compaction; Boudreau, 1997). In addition, both dry sediment and pore fluid are assumed to be buried with an identical velocity at an infinite depth (where $\phi_{f.\ inf}$ is assumed) (Boudreau, 1997). These two assumptions were used to derive burial velocities for dry sediment and pore fluid:

$$v_{f.x} = \frac{U_f}{\phi_{f.x}} = \frac{\phi_{f.inf} v_{inf}}{\phi_{f.x}} \tag{6}$$

$$v_{s.x} = \frac{U_s}{\phi_{s.x}} = \frac{\phi_{s.inf} v_{inf}}{\phi_{s.x}} \tag{7}$$

U_f and U_s: volumetric fluxes of pore fluid/dry sediments;
v_{inf}: burial velocity at an infinite depth (row (e) in Table 2).

When necessary, an additional advective velocity for pore fluid was assigned:

$$v_{ext.x} = -p v_{f.x} \tag{8}$$

p: a positive scaler.

We assumed strontium is only consumed by authigenic carbonate formation and produced through the decomposition of VA. For the formation of authigenic carbonate, we formulated the reaction term for the carbonate phases in Eq. (2) as:

$$\Psi \phi_{f.x} k_c S_x^t \frac{1}{\Gamma_C} \tag{9}$$

Ψ: an error function determining the depth of reaction occurrence (controlled by R_{carb1} and R_{carb2}, rows (j) and (k) in Table 2);
k_c: kinetic constant for carbonate precipitation (1/yr, row (i) in Table 2);
Γ_C: mole of strontium in every gram of carbonate (calculated from row (n) in Table 2).

The Sr/Ca molar ratios in carbonates, and thus Γ_C, depend on the type of carbonate in the sediments. In general, calcites have ratios in the range of sub mmol/mol (Baker et al., 1982) and aragonites could have ratios an order of magnitude higher (Joseph et al., 2013b). Other carbonates, such as siderite and Mn-carbonate have an order of magnitude lower strontium content compared to calcite (Cortecci and Frizzo, 1993; Kuznetsov et al., 2005; Phillips et al., 2018). We adopted values between 3.1 and 4.5 mmol/mol for all sites investigated except for Site C0020 where strontium content in the carbonate is available (~200 ppm; Phillips et al., 2018) (Table 2). For VA alteration, the reaction term was formulated as:

$$k_A A_x^t \phi_{s.x} \tag{10}$$

k_A: kinetic constant for VA alteration (1/yr, row (l) in Table 2);
A_x^t: gram of VA in dry sediments as a function of depth and time.

The reaction term for pore fluid in Eq. (3) was formulated as:

$$-\Psi\phi_{f.x}k_c S_x^t + k_A A_x^t \phi_{s.x}\Gamma_A \tag{11}$$

Γ_A: mole of strontium in VA (mole Sr/g VA) (calculated from row (m) in Table 2).

We uniformly adopted a Γ_A value of 400 ppm for the four sites investigated. Strontium content in volcanic glass varies wildly from a few hundred ppm (Cao et al., 1995; Sutton et al., 1995; Wilson et al., 2006) to sub-percent level (Valle et al., 2010; Parruzot et al., 2015). This value will not affect the rate determined by the model as the amount of strontium required is strictly constrained by the overall mass balance. With a smaller Γ_A, more VA is needed to be buried from the seafloor to reach the mass balance (see *Discussion* for the difference between volcanic glass and VA). We assumed no authigenic carbonate at the seafloor and variable VA abundance for the top boundary condition (Table 3). Eq. (11) was applied to pore fluid calcium to additionally constrain the Ca/Sr molar ratios in VA with the values listed in Table 3. For pore fluid strontium, the top boundary condition was set to be a function of time to reflect the changes in seawater strontium isotopic ratios (Veizer, 1989):

$$\left(\frac{^{87}Sr}{^{86}Sr}\right)_{t1}^{t2} = 0.70920 - 3.75 \times 10^{-11}t,\ t_1 = 0\ and\ t_2 = 40\ Ma \tag{12}$$

$\left(\frac{^{87}Sr}{^{86}Sr}\right)_{t1}^{t2}$: $^{87}Sr/^{86}Sr$ ratio of seawater as a function of time.

The temporal variation of seawater strontium concentration is only poorly constrained (Vollstaedt et al., 2014; Pearce et al., 2015). We assumed a monotonical decrease in seawater strontium concentrations from 130.2 μM to 86.6 μM between the oceans 70 Ma ago and present day, respectively (Steuber and Veizer, 2002). See Fig. S2 from *Supplementary materials* for a demonstration of how seawater burial influences the strontium system in pore fluid. For the bottom boundary condition of pore fluid strontium, we assigned no flux boundaries assuming no exchange of strontium deeper than the modeled depth. We assumed that ^{86}Sr, ^{87}Sr, and ^{88}Sr are the only three isotopes in the strontium system and applied Eqs. (2) and (3) separately on each of them. We assumed the fraction of ^{88}Sr in the seawater to be constant (83.13%) with time. Isotopic fractionation factor for ^{88}Sr (with respect to ^{86}Sr) during carbonate precipitation is set to be 0.176‰ (Vollstaedt et al., 2014). VA alteration releases strontium with a constant $\delta^{88}Sr$ signal (0.4‰ or a $^{88}Sr/^{86}Sr$ molar ratio of 8.37521; Hoefs, 2009). See *Supplementary materials* for sensitivity tests with respect to the changes in $\delta^{88}Sr$ (Fig. S1). We solved Eqs. (2) and (3) numerically with the Crank-Nicolson scheme (i.e., implicit in time and equal weight for adjacent space nodes). We however formulated reaction terms with an explicit fashion to avoid potential stiff conditions when reactions are fast. Spatial and temporal discretization was determined at the different study sites depending on the depth and time scales of interest (rows (c) and (d) in Table 2).

3.2. Constraints and uncertainties of the model

The sources of all data used for constraining the model were shown in Table S1. Porosity and sedimentation rates are essential to establish the downcore burial velocities for both the solid phases and pore fluid. Due to sediment compaction, downcore sediment burial velocity is not constant with depth. It is therefore difficult to simply estimate such velocity from the age of the sediments. We determined this by choosing a v_{inf} value (Eq. (7)) so that a sediment parcel can be buried to the desired depth at the time based on the observed age information and downcore porosity trend. Burial velocity for pore fluid was calculated in a similar fashion using Eq. (6). Fluid burial velocity always has the same sign but lower magnitude as the burial of the sediment parcel. As a result, pore fluid is always advectively transported downward relative to the seafloor (i.e., zero depth) but upwardly transported relative to the sediment at the same depth. External fluid ascending velocity ($v_{ext.f}$) can be constrained from the pore fluid profiles, but it is assumed absent at all investigated sites.

After constraining the strontium transport, the remaining unknowns are reaction rates and depth ranges where alteration of VA and carbonate formation occur. We assumed that carbonate dissolution does not occur at any of the four sites investigated. Such assumption therefore limits the applicability of this model to locations with no significant release of strontium from carbonate dissolution. As demonstrated by sensitivity tests (see *Supplementary materials*, Figs. S3–S5), the concentrations of strontium and calcium in pore fluids combined with the $^{87}Sr/^{86}Sr$ profiles can provide enough constraints to quantify both reactions. As an additional constraint, when available, we use the

Table 3
Model output.

Variable	Unit	Nankai Trough C0012	Tuaheni GeoB20802	Costa Rica U1413	Shimokita C0020
Asymptotic pore fluid $^{87}Sr/^{86}Sr$	mol/mol	0.70600	0.70843	0.70700	0.70600
Model-estimated $^{87}Sr/^{86}Sr$ in VA	mol/mol	0.70580	0.70815	0.70700	0.70600
Assigned Sr/Ca for VA in model	mmol/mol	4.54	4.54	4.54	4.54
Seafloor VA content	dry wt%	13	6	2	6[a]
Range of Sr release rates through VA decomposition	nmol Sr/m^3 bulk sed/yr	10^1 to 10^2	10^3	$10^{1.2}$	10^1
Range of Sr consumption rate through carbonate precipitation	nmol Sr/m^3 bulk sed/yr	$10^{0.5}$ to 10^3	10^3 to $10^{3.5}$	0 to 10^3	10^0

[a] Seafloor VA content between 20 and 29 Ma.

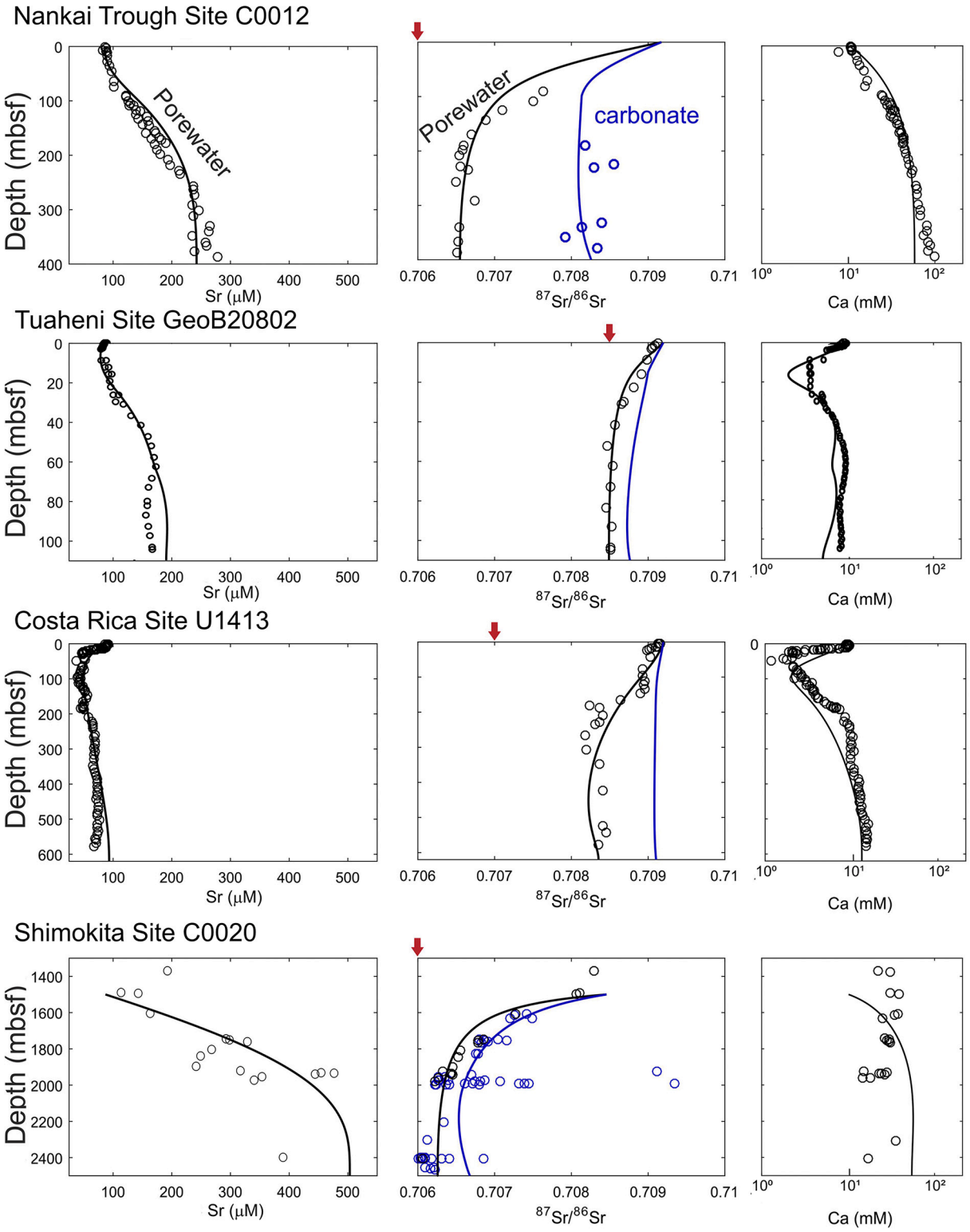

Fig. 3. Model results and the pore fluid data of strontium concentration, $^{87}Sr/^{86}Sr$ ratio, and calcium concentration. The black lines are model results for pore fluids while blue lines indicate modeled $^{87}Sr/^{86}Sr$ ratios of carbonates. Black open circles are pore fluid data while blue open circles are $^{87}Sr/^{86}Sr$ data for carbonates (only available for Sites C0012 and C0020). See Table S1 for the references of the data used. The red arrows mark the model-derived $^{87}Sr/^{86}Sr$ ratios for VA at each location investigated, which in all cases are substantially higher than the ratios reported for volcanic glass (see Fig. 5 for comparison). (For interpretation of the references to color in this figure legend, the reader is referred to the web version of this article.)

presence of authigenic carbonates and/or the $^{87}Sr/^{86}Sr$ ratios of authigenic carbonates to further quantify authigenic carbonate formation. This was only possible for Sites C0012 and C0020 as no carbonate nodules/concretions were recovered from U1413 and GeoB20802. Once the rate and depth range of carbonate precipitation can be satisfactorily constrained, we can uniquely quantify the rates of VA alteration at each of the investigated sites.

Model results for Site C0020 may be subject to large uncertainties as

the strontium data from the first 1500 m of sediments were not sampled. The available data only allow us to model the evolution of the strontium system from 29 Ma to 20 Ma (Phillips et al., 2016); which provides an old end-member example among the studied sites. In addition, the observed porosity trend does not represent the porosity during the time window modeled. Instead, we fit the porosity profile for the first 400 m of sediments as reported by Tomaru et al. (2009) and assumed that this represents the porosity for the required time span. This assumption is reasonable as long as steady-state compaction is valid at this site.

4. Results

The downcore profiles for pore fluid strontium and calcium together with the best-fit results from our model are shown in Fig. 3. The pore fluid strontium concentrations vary by a factor of six among the four locations investigated. Site C0020 (Shimokita) has the highest concentration (up to ca. 450 μM) whereas the highest strontium concentration from Site U1413 (Costa Rica) reaches only ~75 μM or slightly lower than the seawater value. The downcore trends of dissolved strontium concentration from the four locations are also different. At Site U1413, the upper 100 m of sediments show a decrease in strontium concentration with depth; the concentration gradually increases between 100 and 300 mbsf and maintains at a similar level below 300 mbsf. The highest strontium concentration at GeoB20802 (Tuaheni) reaches ca. 170 μM. A concave upward concentration profile above 60 mbsf is observed at this location. The concentration fluctuates between 150 and 170 μM from 60 to 110 mbsf. Strontium concentration reaches 275 μM at 400 mbsf of Site C0012 (Nankai Trough) showing an overall increasing trend downhole. A closer look of the profile reveals that the downhole increase in strontium concentration in the first 50 m of sediments is less obvious compared to the deeper sediments. Between 100 and 300 mbsf, strontium concentration increases from ca. 100 to 250 μM. The concentration fluctuates between 240 and 270 μM from 300 to 400 mbsf at Site C0012. The sediments deeper than 400 mbsf are known to be affected by the fluid interaction with crustal basement (Joseph et al., 2013a; Torres et al., 2015) and are not considered in our present modeling. At Site C0020, the strontium concentration shows more fluctuation compared to all the other sites investigated. However, a general downhole increasing trend can be observed with the deepest sample at 2406 mbsf showing 382.9 μM of strontium. The three samples between 1936.8 and 1944.5 mbsf, which correspond to the depth range where a major coal bed was recovered (Gross et al., 2015), have strontium concentrations over 450 μM (Fig. 3). Despite the high strontium concentration of these three samples, variation in $^{87}Sr/^{86}Sr$ ratios is rather small.

The dissolved calcium concentration profiles from all sites are seemingly similar to the strontium profiles (Fig. 3). Nonetheless, the range of variation in the concentrations of both solutes, relative to their seawater values, are quite different. At Site U1413, despite the similar structure in the profiles of calcium and strontium, calcium concentration is ~1.5 times higher than seawater concentration below 500 mbsf, while strontium is always lower than seawater concentration throughout the cores. In contrast, at Site GeoB20802, the calcium concentration is never higher than seawater throughout the 110 m of sediments recovered, whereas the strontium concentration reaches almost twice the seawater value. The overall profiles of calcium and strontium from GeoB20802 are also different, with an obviously low calcium concentration (ca. 3 mM) between 10 and 30 mbsf where the strontium concentration increases steadily. At Site C0012, despite the similar overall downcore trend, calcium concentration reaches 20 times of the seawater value, whereas strontium concentration is only ca. 4 times higher than seawater (Fig. 3). At Site C0020 the calcium concentration profile exhibits rather large variation and no apparent downcore structure, which has been attributed to contamination with drill mud (Expedition 337 Scientists, 2013a). The similar overall structure of the downcore profiles for calcium and strontium but different concentration ranges at these four sites suggest different reaction rates and Ca/Sr ratios for the solid phases considered.

Despite the different strontium concentration profiles observed, the pore fluid $^{87}Sr/^{86}Sr$ profiles have similar downcore trends but different asymptotic ratios among the four sites (Table 3 and Fig. 3). Mixing between modern seawater values and fluids containing low $^{87}Sr/^{86}Sr$ can generally be observed from the upper half of the profiles at all locations. For the lower half of the profiles, the $^{87}Sr/^{86}Sr$ ratios approach 0.70850 at Site GeoB20802, 0.70840 at Site U1413, 0.70650 at Site C0012, and 0.70600 at Site C0020 (Fig. 3). The similar downcore trends and the low $^{87}Sr/^{86}Sr$ ratios at the four locations support the interpretation that VA alteration is the common process driving the changes in pore fluid strontium isotopic ratios at these locations (Elderfield and Gieskes, 1982; Moen et al., 2015; Torres et al., 2015; Phillips et al., 2018). We however note that the asymptotic ratios from Sites C0012, GeoB20802, and U1413 (Table 3) are significantly higher than the ratios reported for volcanic glass at these locations (0.70355–0.706798 from Costa Rica, Schindlbeck et al., 2016a; 0.70551–0.70601 from New Zealand, Sutton et al., 1995; Wilson et al., 2006; 0.70368 from Nankai Trough, Kutterolf et al., 2014; no such data are available for Site C0020).

We acknowledge that the model does not adequately simulate the pore fluid calcium data at all sites; whereas the fit for Sites C0012 and U1413 seems reasonable, C0020 and GeoB20802 are less good. In the case of C0020, the calcium data reflects drill fluid contamination, as acknowledged in the expedition report (Expedition 337 Scientists, 2013b). The reason for the discrepancy for Site GeoB20802 is less clear which maybe partly due to the constant Sr/Ca ratios of carbonate and VA phases assigned in the model (Γ_C in Eq. (9) and Γ_A in Eq. (11), respectively). In reality, these ratios may vary with depths and time. Other sources of dissolved calcium, such as the calcium from the basement fluids that influence Site C0012 (Torres et al., 2015), which is not considered in the current model, may also contribute to the discrepancy between the modeled and observed calcium profiles. Notwithstanding these discrepancies, in all cases our model yielded a good fit to the measured pore fluid strontium concentrations and $^{87}Sr/^{86}Sr$ ratios (Fig. 3). Additional constraints from the $^{87}Sr/^{86}Sr$ of authigenic carbonates were also considered when modeling the profiles from Sites C0012 and C0020 (Fig. 3). The VA alteration rates at the four locations vary between 10^1 and 10^3 nmole $Sr/m^3/yr$ (Fig. 4). A similar range of carbonate precipitation rate (with respect to strontium consumption) was also estimated (Fig. 4). When comparing the two rates at a given location, strontium is released through VA alteration faster than carbonate precipitation from Sites C0012 and C0020 and therefore results in the accumulation of strontium in the pore fluid. At Site U1413, the high rate of carbonate precipitation was inferred from the low strontium concentration in the first two hundred meters of sediments. Despite the highest rates estimated from the Site GeoB20802 (Fig. 4), the strontium concentration in pore fluid is not as high as that from the other locations indicating much of the strontium released from VA alteration is consumed by carbonate precipitation. Our model also generates a $^{87}Sr/^{86}Sr$ ratio corresponding to the VA at each site; these values range from 0.70600 (Sites C0012 & C0020) to 0.70843 (Site GeoB20802) (Table 3); they are lower than the asymptotic ratios read from the pore fluid profiles (Fig. 3) but substantially higher than the ratios reported for volcanic glass at each respective site (Fig. 5 and Table 3).

5. Discussion

By considering the strontium mass balance among the pore fluid, authigenic carbonate, and VA phases, we quantified the rates of associated reactions as well as the $^{87}Sr/^{86}Sr$ ratios for the VA being altered. In the following sections, we provide interpretations on the $^{87}Sr/^{86}Sr$ ratios in the pore fluid relative to the reported isotopic ratios for

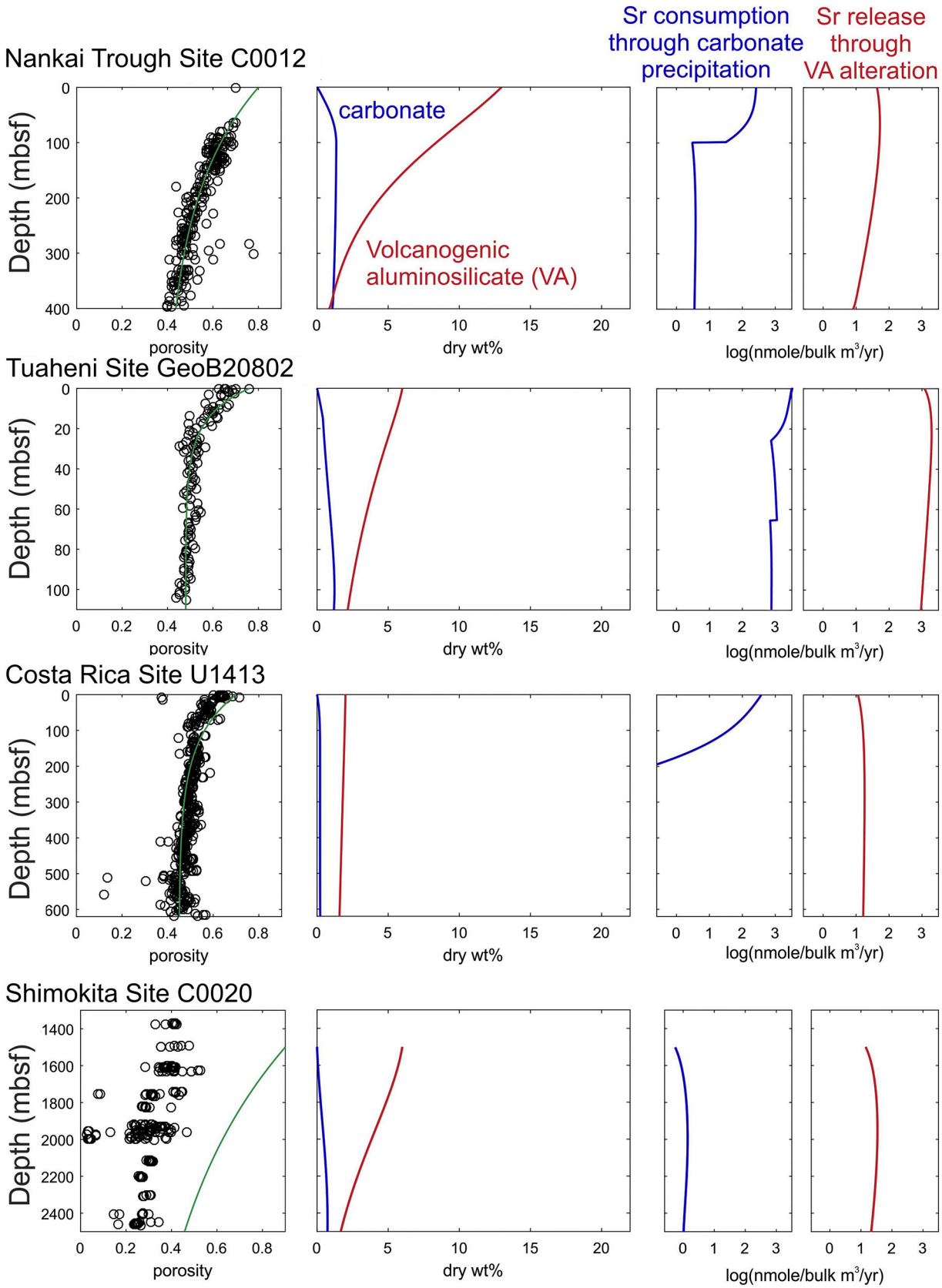

Fig. 4. The model-derived contents of carbonate and VA (in dry wt%) as well as the strontium consumption and releasing rates. The porosity downcore profiles fitted as model input at each site were also shown (see Table S1 for the sources of porosity data). For Site C0020, the porosity profile for the first 400 m of sediments from Tomaru et al. (2009) was assumed to represent the porosity of the time span considered in the model.

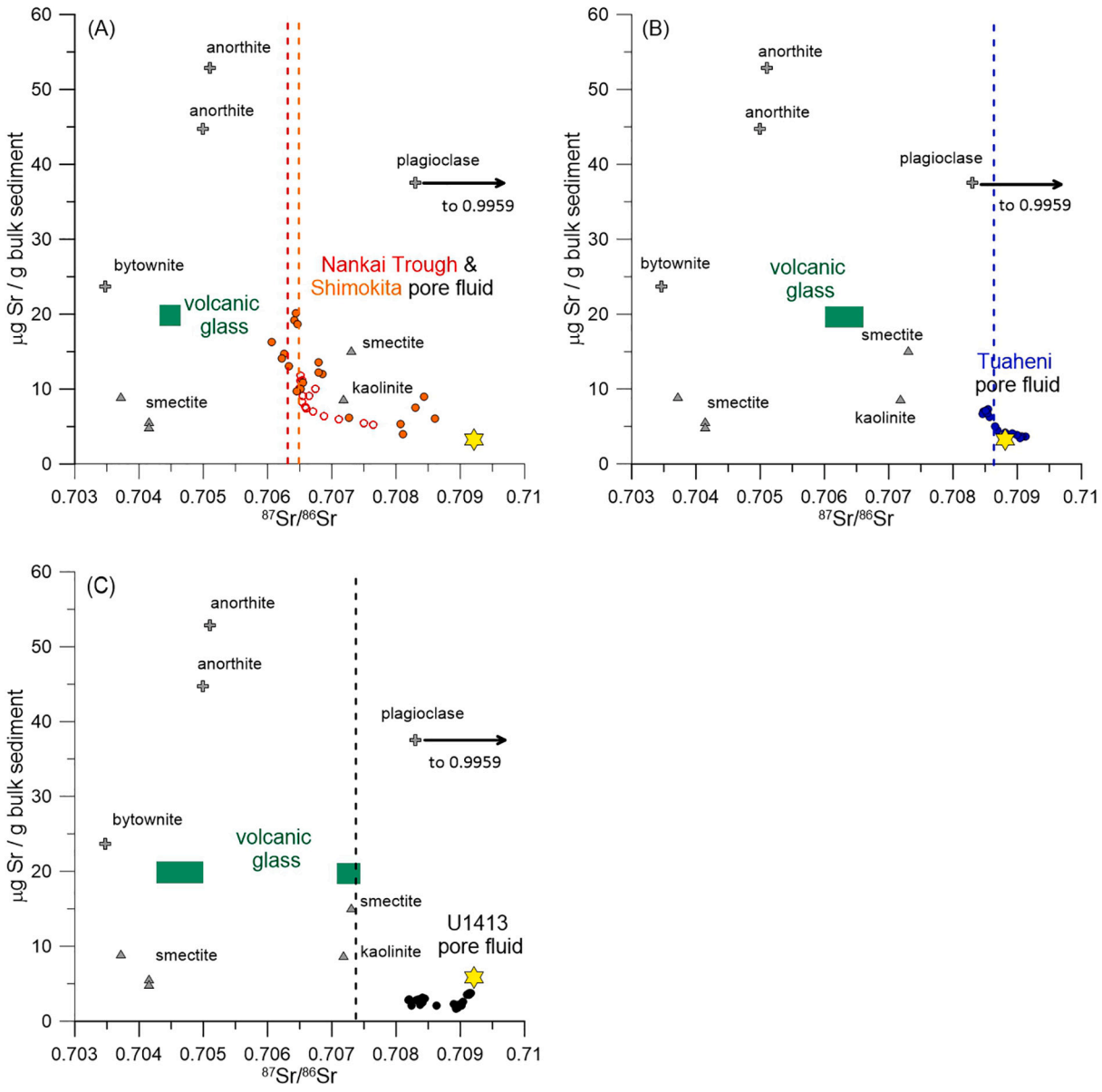

Fig. 5. Summary of $^{87}Sr/^{86}Sr$ ratios in various silicate minerals (grey symbols), pore fluids (open and closed circles), and modern seawater (yellow stars) for the four investigated sites. The ratios from volcanic glass are from literature (Schindlbeck et al., 2016a for U1413, Kutterolf et al., 2014 for Nankai Trough and Sutton et al., 1995 for Tuaheni). See text for the references of other silicate minerals. The sources for pore fluid $^{87}Sr/^{86}Sr$ data are summarized in Table S1. $^{87}Sr/^{86}Sr$ ratios for volcanic glass (green squares) from C0012 and C0020 (A; $n = 1$), GeoB20802 (B; $n = 3$) and U1413 (C; $n = 15$) were included to compare with the model-derived $^{87}Sr/^{86}Sr$ ratios for VA (dash lines). To compare the strontium concentration from the different media, we assumed the abundance of feldspar, clay, and volcanic glass is 10 wt% of dry sediments and porosity is 50%. The ratio of feldspar (microcline) can be as high 0.99590 (Brantley et al., 1998) which is not included in the plot. Our model estimates higher $^{87}Sr/^{86}Sr$ ratios for VA when compared to the volcanic glass. (For interpretation of the references to color in this figure legend, the reader is referred to the web version of this article.)

volcanic glass and discuss the impact of VA alteration on elemental cycles.

5.1. Source of strontium in pore fluid

Evidently, the pore fluid data at the four investigated sites suggest a mixture of buried seawater strontium with strontium released with a deficit in ^{87}Sr from volcanogenic material alteration (Fig. 3). However, even at great depth, pore fluid never reaches the low $^{87}Sr/^{86}Sr$ ratios reported on volcanic glass measurements at each site (Fig. 5). Likely explanations for such discrepancy include: 1) volcanic glass are highly heterogeneous; therefore, the reported $^{87}Sr/^{86}Sr$ might not reflect the full range of ratios for volcanic glass; 2) the higher ratios in pore fluid reflect substantial mixing with the buried seawater even at great depth; 3) volcanic glass is not the only source of strontium; rather, other reactive silicate minerals in the sediments may also undergo alteration; and 4) authigenic clays forming from alteration of volcanic glass incorporate strontium with unique $^{87}Sr/^{86}Sr$ ratios leading to changes in the observed pore fluid data. We show in the following discussion that alteration of silicate minerals and/or formation of clay minerals, in additon to volcanic glass alteration, are needed to explain the discrepency in $^{87}Sr/^{86}Sr$ ratios.

Indeed, volcanic glass distributed in the sediment can be heterogeneous and thus a definite endmember $^{87}Sr/^{86}Sr$ ratio may be difficult to define. This is not because of the heterogeneous amorphous nature of the volcanic glass itself since isotope values from one eruption and one

volcanic center location are normally very homogenous. Rather, this results from the wide dispersal range (up to 1000 km) of volcanic glass provenance and therefore the possible contribution of a larger range of isotopic signatures along the volcanic arc (e.g., Carr et al., 2003). The 15 measurements of volcanic glass from Site U1413 show values that mostly cluster around 0.70396 (n = 14; σ = 0.000536) with one exceptional large ratio of 0.70680 (Schindlbeck et al., 2016a) (Fig. 5), which is still lower than the asymptotic ratio in pore fluid. The $^{87}Sr/^{86}Sr$ ratios of lava/pumice from the Taupo volcano, New Zealand, can be as high as 0.70721 (Sutton et al., 1995) but still much lower than the ratio in pore fluid from Site GeoB20802. We therefore conclude that, despite the heterogeneity in volcanic glass, the $^{87}Sr/^{86}Sr$ ratios in pore fluids are significantly higher than the overall isotopic ratios in volcanic glass.

Seawater of different ages contributes significantly to the pore fluid. By simulating the evolution of pore fluid strontium solely due to seawater burial for 29 Ma (Fig. S2), we show that pore fluid $^{87}Sr/^{86}Sr$ can be as low as 0.70810 at 1000 mbsf. Such downcore variation in $^{87}Sr/^{86}Sr$ ratios can only partly explain the observed ratios from the pore fluid profiles. Such results indicate that a release of strontium from VA alteration with $^{87}Sr/^{86}Sr$ ratios ranging from 0.70580 to 0.70815 is indeed required to explain the observed downcore trend at the four sites (Fig. 3 and Table 3).

The higher $^{87}Sr/^{86}Sr$ ratios derived for VA in our model, compared to volcanic glass reported at each location (Fig. 5), suggest a strontium contribution from other minerals. VA, defined as volcanic matter derived from eruptions, includes not only volcanic glass but also "phenocrysts" (crystals that grow within the magma chamber). It is known that VA and especially tephra layers can include substantial amount (1 to up to 50 vol%) of crystals such as feldspar, pyroxene, amphibole, biotite, spinel and apatite; crystal-rich zones particularly occur at the base of coarse ash beds (e.g., Kutterolf et al., 2008a; Schindlbeck et al., 2016a). Even more, reworking of tephra layers distributes VA in the marine sediments that harbor detrital silicates and, if transported in form of turbidites downslope, often concentrates VA in marine sediments as layers. For comparison, we compiled $^{87}Sr/^{86}Sr$ ratios from feldspar and clay minerals in Fig. 5. Plagioclase (including feldspar, albite, anorthite, bytownite, and microcline) has very high strontium content (from several hundred to over a thousand ppm) with $^{87}Sr/^{86}Sr$ ratios higher but close to seawater and pore fluid values (0.70347–0.99590; Fig. 5) (Heier and Compston, 1969; Clauer, 1981; Brantley et al., 1998; White et al., 2001). Clay minerals formed from the weathering of volcanic glass and basalt have $^{87}Sr/^{86}Sr$ ratios close to or lower than the pore fluid ratios (0.70370–0.70730; Fig. 5) (Dasch, 1969; Clauer, 1979). Biotite, muscovite, and phlogopite, though were not included in Fig. 5, can also be found in association with volcanic glass and may be especially important for Site U1413, where significant amount of biotite was detected. These minerals are characterized by very high $^{87}Sr/^{86}Sr$ ratios ($2-10$) with strontium concentration lower than plagioclase and clay minerals ($<$tens of ppm) (Heier and Compston, 1969; Clauer, 1981; Taylor et al., 2000; White et al., 2001).

If we assume that VA is composed of primarily volcanic glass (VG) and feldspar, we can determine the fraction of the two through a binary mixing calculation (Fig. 6A):

$$(^{87}Sr/^{86}Sr)_{model-VA} = (^{87}Sr/^{86}Sr)_{VG} \times f_{VG} + (^{87}Sr/^{86}Sr)_{feldspar} \times f_{feldspar}$$
$$f_{VG} + f_{feldspar} = 1$$

As a result, 5–25 wt% of feldspar (or 2.7–13.7 vol% assuming a density for feldspar of 2.56 g/cm^3) in the bulk VA can explain the ratios our model derived for Site GeoB20802 ($f_{feldspar}$ = 0.05 to 0.25; Fig. 6A). Such a range of feldspar abundances is more than plausible since even marine background sediments have feldspar contents of 10–20 wt% evident from XRD analyses of Site C0012 sediments (Expedition 333 Scientists, 2012). Additionally, smear slide observations from Site U1413 indicate abundant feldspars (10–25 vol%) within the entire sediment sequence (Harris et al., 2013b). Taking into account that tephra layers and turbidites have crystal contents of up to 50 vol%, with feldspar having by far the highest portion (Kutterolf et al., 2008a; Kutterolf et al., 2018), the overall ~3 to 14 vol% of feldspar, needed to explain the ratios of the model, is feasible.

In an alternative view, the strontium released from VA could be the net effect of volcanic glass dissolution and the consequential clay mineral formation. Authigenic clay minerals that form as a result of volcanogenic silicate alteration are known to have low $^{87}Sr/^{86}Sr$ ratios (Fig. 5). The relative contribution of the two reactions can also be estimated following:

$$(^{87}Sr/^{86}Sr)_{model-VA} = (^{87}Sr/^{86}Sr)_{VG} \times f_{VG} - (^{87}Sr/^{86}Sr)_{clay} \times f_{clay}$$
$$f_{VG} - f_{clay} = 1 \quad (13)$$

Through such calculation, the model-derived $^{87}Sr/^{86}Sr$ for Site GeoB20802 can be matched when 55 to 65 wt% of the strontium from volcanic glass dissolution is consumed by clay formation (Fig. 6B). Such an estimation is however higher than the estimation by Yokoyama and Banfield (2002) who concluded that clay formation is responsible for 20 wt% uptake of volcanic-glass-derived silica. Our current strontium mass balance approach is not able to differentiate the two reactions (i.e., feldspar dissolution vs. clay mineral authigenesis). It is likely that the both reactions play a role in the sediments where dissolution of volcanic glass is currently active. By extending the binary mixing to a tertiary mixing, we can demonstrate the relative contribution from the three processes:

$$(^{87}Sr/^{86}Sr)_{model-VA} = (^{87}Sr/^{86}Sr)_{VG} \times f_{VG} + (^{87}Sr/^{86}Sr)_{feldspar} \times f_{feldspar} - (^{87}Sr/^{86}Sr)_{clay} \times f_{clay}$$
$$f_{VG} + f_{feldspar} - f_{clay} = 1 \quad (14)$$

To match the 20 wt% of strontium uptake by clay minerals (Yokoyama and Banfield, 2002), we assumed that 23 wt% of the strontium is consumed by clay formation ($f_{clay}/(f_{VG} + f_{feldspar}) = 0.23$), and arrive at a model-derived high $^{87}Sr/^{86}Sr$ ratio from Site GeoB20802 with a 3–20% strontium contributed from feldspar dissolution ($f_{feldspar}/f_{VG}$ = 0.03–0.2. The actual contribution of the three processes is currently unknown, but our result of 3–20 wt% contribution from feldspar is feasible considering the overall feldspar content of the sediment. A comprehensive consideration that include more pore fluid data and detailed petrographic sediment analyses will be required to determine the relative importance of these reactions. It is therefore important to emphasize that the VA alteration rates estimated from our model are effective rates that represent the summation of these silicate phases.

5.2. VA alteration: comparison with field observations and lab experiments

From the previous discussion, the VA as defined here is likely an assemblage of different volcanogenic silicates with volcanic glass being the major component. Therefore, a direct comparison between the abundance of VA estimated from our modeling (Fig. 4) and the volcanic glass estimated from visual inspection (Fig. 2) is only correct to the first order. Nonetheless, such comparison is important to verify the feasibility of the mass balance considered. For Sites C0012 and C0020, our model indicates that alteration of 13 and 6 wt% of VA over 20 and 9 Ma, respectively, is required to satisfy the mass balance (Fig. 4). This corresponds to 9.6 and 4.5 vol% assuming density for bulk sediment and volcanic glass are 1.78 and 2.4 g/cm^3, respectively, at Sites C0012 and C0020 (Underwood et al., 2010). The volcanogenic materials (volcanic glass, tephra, and pumice) in the sediments between 600 and 2500 mbsf at Site C0020 vary from common (1–10 vol%) to few (0.1–1 vol%) with discrete layers of abundant (10–50 vol%) glass (Fig. 2) (Expedition 337 Scientists, 2013a). Similarly, at Site C0012, volcanic glass content ranges in average between 10 and 30 vol%, with occasion layers with >60 vol% of glass (Fig. 2) (Scudder et al., 2018).

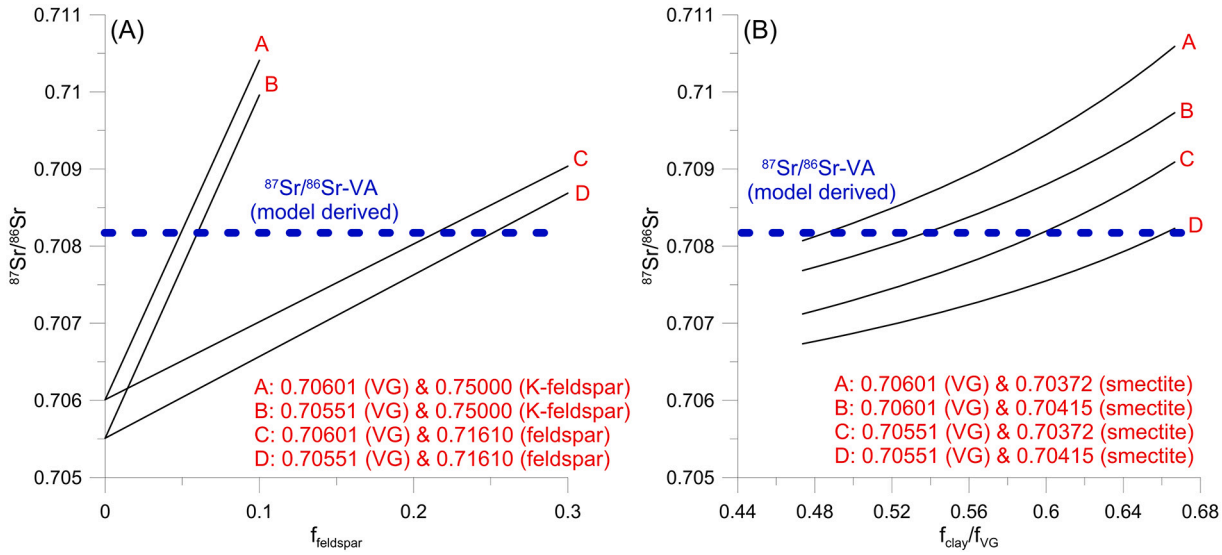

Fig. 6. Binary mixing of (A) dissolution of volcanic glass and feldspar and (B) volcanic glass (VG) dissolution and clay formation. The calculation was done by using Site GeoB20802 as an example, the site with the highest model-derived $^{87}Sr/^{86}Sr$ ratio for VA.

These semi-quantified abundances of volcanic glass suggest that our estimated amounts of VA being altered are reasonable. It is important to note that the model-derived VA abundance can only be interpreted on a relative base, and that our model assumes a steady input of VA from the seafloor, which is not always the case as episodic volcano eruptions and consequential sudden inputs of VA are likely. Rather, our model results should be deemed as a long-term average of VA alteration.

The effective VA alteration rates, as derived from our mass balance approach, include rates of volcanic glass dissolution, feldspar (or other abundant silicate minerals in bulk VA) dissolution, and/or clay mineral authigenesis. We deem such bulk reaction rate represents a suitable estimation towards the assessment of VA alteration on a global scale as these processes often occur simultaneously in sediments rich in volcanic glass. For the four locations investigated, Site GeoB20802 has the highest VA alteration rate (~10^3 nmole Sr/m^3/yr; Fig. 4) whereas the other three locations have similar overall rates (10^1 to 10^2 nmole Sr/m^3/yr; Fig. 4). The young sediment, and therefore the very reactive VA, from Site GeoB20802 (110 ka, Table 2) may explain the high alteration rate estimated as compared to other sites. The active VA dissolution across such wide temporal (110 ka to 29 Ma ago) and spatial scales provides an indication of the global significance of this reaction over geological time scales.

Rate of volcanic glass dissolution has been quantified previously through laboratory experiments, field observations, and numerical methods (Table 1). Comparing our results with these quantifications, however, faces several main challenges. First of all, most of these previous quantifications are silica-based rates that are normalized to the surface area (or weight) of volcanic glass. In other words, to compare with our model-derived results, one needs to know the silica-to-strontium ratio in volcanic glass, the surface area (or weight) of volcanic glass, and the content of volcanic glass in bulk sediments, under the assumption that VA is mainly composed of volcanic glass. Secondly, as we elaborated previously, the rates derived from our mass balance approach represent the summation of several reactions that occurred simultaneously during volcanic glass dissolution. Third, most of the previous studies focus on volcanic glass dissolution over the time scale of millennium at most, which is substantially shorter than the ages of sites investigated by this work (except for Site GeoB20802).

Despite these obvious limitations, we attempted to compare our results with the volcanic glass dissolution rates determined from field observations by Yokoyama and Banfield (2002). Based on the decreasing trend of silica content in outcrops of different ages (up to 52,000 years), they estimated a rate of ca. $10^{-18.22}$ mol Si/cm^2 (volcanic glass)/sec (Table 1). If we take our result from Site C0012 as an example, use our estimated average VA alteration rate of $10^{-7.48}$ mol Sr/m^3 (bulk sediment)/year (Fig. 4), and assume bulk sediment density of 1.78 g/cm^3 (Underwood et al., 2010), a Si/Sr molar ratio in volcanic glass of 4294 (Cao et al., 1995), 13 wt% of volcanic glass in bulk sediments (based on the decrease of our modeled VA abundance; Fig. 4), and a volcanic glass surface area of 0.24 m^2/g (Yokoyama and Banfield, 2002), we arrive a rate of $10^{-20.09}$ mol Si/cm^2 (volcanic glass)/sec, or almost two orders of magnitude lower than what is determined by Yokoyama and Banfield (2002).

Large uncertainties are however associated with this calculation. For example, the derived 13 wt% decrease in VA depends on the strontium content in VA we assigned in the model (row (m) in Table 2) with less VA needed if the strontium content in VA is higher. Surface area of volcanic glass also subjects to large uncertainties and depends on factors such as grain size, the method used, and the type of glass. A variation of an order of magnitude is highly possible (e.g., Yokoyama and Banfield, 2002). Besides the associated uncertainties, another likely explanation is the different time scales used in their estimations compared to ours. As pointed out by a later study (Yokoyama, 2013), volcanic glass dissolution rate is time-dependent as the glass loses its activity with time. If we extrapolate the equation derived by Yokoyama (2013) from their 277-day experiment to 20 Ma, we arrive at a rate of $10^{-20.284}$ mol Si/cm^2 (volcanic glass)/sec, which is similar to our model-derived rate for Site C0012. Pressure is another factor that may contribute to the difference in the rates estimated (Schacht, 2005) as the VA from Site C0012 must have experienced much greater pressure compared to the onshore volcanic glass reported by Yokoyama and Banfield (2002).

5.3. Authigenic carbonate precipitation as a result of VA alteration

Authigenic carbonate precipitation triggered by VA alteration has been documented in several recent studies. Clumped isotope analyses of the carbonates recovered from Site C0012 document carbonate formation at depth (Sample et al., 2017). The $^{87}Sr/^{86}Sr$ ratios of these carbonates represent a mixture of strontium derived from seawater and pore fluids that carry a signal of VA alteration (Fig. 3). For Site C0020 recovered from Shimokita, the $^{87}Sr/^{86}Sr$ ratios in the carbonates are as low as the ratios from co-located pore fluid samples (Fig. 3) suggesting in-situ formation of these carbonates and the incorporation of dissolved

strontium modified by VA alteration (Phillips et al., 2018). Torres et al. (2020) summarized observations from several locations around the world showing that authigenic carbonate precipitation in deep sediment sequences is driven by the increase in alkalinity and dissolved cations that result from weathering of silicate minerals, including VA.

Similar to the model-derived VA abundance, we can only confidently estimate the relative amount of authigenic carbonate precipitated but not the absolute abundance of carbonate in the sediments. Our model indicates that less than ~2 wt% of VA-associated authigenic carbonate precipitated at the four locations investigated. We therefore do not expect large concretions of carbonate to form in the sediments as a result of VA alteration. Most of these authigenic carbonate minerals are likely disseminated in the sediments. The carbonate nodules found from the sediments of Nankai Trough and Shimokita are mixtures of carbonates formed at much shallower depths as well as those formed in association with VA alteration (Sample et al., 2017; Phillips et al., 2018). At Sites GeoB20802 and U1413, no visible authigenic carbonate nodules were found (Harris et al., 2013a, Huhn, 2016). Though the absence of detectable carbonate nodules does not necessary support the low percentage of carbonate estimated from our model, our results suggest that precipitation of a small amount of carbonate is sufficient to satisfy the overall strontium mass balance. Some of the massive carbonate concretions in marine sediment are the result of precipitation at methane seeps. While in some cases these are massive deposits, these are limited to small areas on the seafloor. Carbonates formed from VA alteration occur over wide areas of the seafloor and span much thicker depth sections than the seep carbonate. Thus, even if not apparent as visual concretions or veins, they may contribute to a large fraction of the carbon stored in marine sediment (Torres et al., 2020).

Based on our modeled results, the rate of carbonate precipitation in association with VA decomposition is roughly the same as VA decomposition rate (Fig. 4). In other words, most of the strontium released in the deep sediments is precipitated and retained in the sediments. Not much of the strontium is able to escape the “carbonate trap” in the sediments. This is also apparent from the downcore strontium concentration profiles. There is almost no change in pore fluid strontium concentration from the first 30 and 100 m of sediments at Sites GeoB20802 and C0012, respectively, whereas strontium in bottom seawater even diffuses into the shallow sediments from Site U1413 (Fig. 3). The global significance of silicate-associated authigenic carbonate precipitation has been highlighted by works such as Wallmann et al. (2008) and Torres et al. (2020). The latest estimation suggests that globally $\sim 1.2 \times 10^{12}$ mole C/yr is fixed in authigenic carbonates that is associated with silicate weathering (Torres et al., 2020). The fraction of carbon sequestrated as a result of VA dissolution is unclear. Future work applying similar a mass balance approach as in our study has the potential to provide an estimate for this process.

It is known that the (micro)nutrients and elements released during VA dissolution impact the deep biosphere in the marine sediments. For example, Fisk et al. (1998) demonstrated the association between microbes and weathered basaltic volcanic glass samples that were buried from a few meters to 1.5 km below seafloor. They proposed that glass weathering is likely facilitated by the microbial activity and the microbes benefit from the nutrients released from the alteration process. Through field observations and laboratory experiments, Rogers and Bennett (2004) showed that microbes preferentially colonize and weather manufactured silicate glass containing phosphorus and iron. They hypothesized that microorganisms are able to produce organic ligands to chelate metals such as iron. Henri et al. (2016) conducted in-situ experiment by incubating synthetic basaltic glasses from the Mid Atlantic Ridge. They found enriched iron-oxidizing microbial assemblage associating with glass alteration which confirmed that the Fe(II) in the basalt was the energy source for the micro-organisms. Stranghoener et al. (2018) demonstrated that structurally-bound iron in basaltic glass is more readily utilized by bacteria. A recent work by Luo et al. (2020) demonstrated how anaerobic oxidation of methane is coupled with the reduction of Fe(III) released from VA alteration from Site GeoB20802. The scale of such process is not yet clear, partly due to the lack of quantification for VA alteration and carbon-fixation potential in global marine sediments (Jørgensen and Boetius, 2007).

6. Conclusions

We developed a numerical model based on the mass balance of strontium and its isotopes among pore fluid, carbonates, and volcanogenic aluminosilicates (VAs). We applied this model on four locations that are characterized by significant VA input to quantify the effective rates of VA alteration. We show that the higher $^{87}Sr/^{86}Sr$ ratios observed in the pore fluid, as compared to the ratios from volcanic glass, can be explained by feldspar dissolution and/or secondary clay mineral formation that are associated with volcanic glass dissolution. Despite the challenges in comparing with other rate estimates from field and laboratory experiments, our derived VA alteration rates are consistent with previous estimates for volcanic glass dissolution. Our results also confirm the significance of authigenic carbonate precipitation in association with VA alteration. We emphasize the importance of releasing micro-nutrients, such as iron, from VA alteration. Future effort in applying a similar mass balance approach based on strontium data from a larger geographical area could help assess the global significance of these processes.

Declaration of competing interest

The authors declare that they have no known competing financial interests or personal relationships that could have appeared to influence the work reported in this paper.

Acknowledgements

This research used samples and data provided by the Integrated Ocean Drilling Program (IODP), which is sponsored by the US National Science Foundation and participating countries. WLH received funding from the Research Council of Norway under the funding scheme NORCRUST (project 255150). MET received funding from the US Science Support Program (USSP) and the US National Science Foundation (grant OCE-1557519). KS received funding from German Research Foundation (DFG) with Grants KU2685/1-1, 2-1&2.

Appendix A. Supplementary data

Supplementary data to this article can be found online at https://doi.org/10.1016/j.chemgeo.2020.119743.

References

Arrhenius, S., 1889. Über die Reaktionsgeschwindigkeit bei der Inversion von Rohrzucker durch Säuren. Z. Phys. Chem. 4 (1), 226–248.
Baker, P.A., Gieskes, J.M., Elderfield, H., 1982. Diagenesis of carbonates in deep-sea sediments; evidence from Sr/Ca ratios and interstitial dissolved Sr (super 2+) data. J. Sediment. Res. 52 (1), 71–82.
Bangs, N.L., McIntosh, K.D., Silver, E.A., Kluesner, J.W., Ranero, C.R., 2015. Fluid accumulation along the Costa Rica subduction thrust and development of the seismogenic zone. J. Geophys. Res. Solid Earth 120 (1), 67–86.
Barber, A., Brandes, J., Leri, A., Lalonde, K., Balind, K., Wirick, S., Wang, J., Gélinas, Y., 2017. Preservation of organic matter in marine sediments by inner-sphere interactions with reactive iron. Sci. Rep. 7 (1), 366.
Basile-Doelsch, I., Amundson, R., Stone, W., Borschneck, D., Bottero, J.-Y., Moustier, S., Masin, F., Colin, F., 2007. Mineral control of carbon pools in a volcanic soil horizon. Geoderma 137 (3–4), 477–489.
Boudreau, B.P., 1997. Diagenetic Models and their Implementation: Modeling Transport and Reactions in Aquatic Sediments. Springer, Berlin.
Bowden, S.A., Mohamed, A.Y., Edilbi, A.N.F., Lin, Y.-S., Morono, Y., Hinrichs, K.-U., Inagaki, F., 2019. Modelling the Shimokita deep coalbed biosphere over deep geological time: Starvation, stimulation, material balance and population models. Basin Res. 0 (ja).
Brantley, S.L., Chesley, J., Stillings, L., 1998. Isotopic ratios and release rates of strontium

measured from weathering feldspars. Geochim. Cosmochim. Acta 62 (9), 1493–1500.
Cambray, F.W., Vogel, T.A., Mills, J.G., 1993. Origin of compositional heterogeneities in tuffs of the timber mountain-group - the relationship between magma batches and magma transfer and emplacement in an extensional environment. J. Geophys. Res. Solid Earth 100 (B8), 15793–15805.
Cao, L.-Q., Arculus, R.J., McKelvey, B.C., 1995. Geochemistry and petrology of volcanic ashes recovered from Sites 881 through 884: A temporal record of Kamchatka and Kurile volcanism. In: Proc. ODP, Sci. Results.
Carr, M., Feigenson, M., Patino, L., Walker, J., 2003. Volcanism and geochemistry in Central America: Progress and problems. Geophys. Monogr. Am. Geophys. Union 138, 153–174.
Clauer, N., 1979. Relationship between the isotopic composition of strontium in newly formed continental clay minerals and their source material. Chem. Geol. 27 (1–2), 115–124.
Clauer, N., 1981. Strontium and argon isotopes in naturally weathered biotites, muscovites and feldspars. Chem. Geol. 31, 325–334.
Clift, P., Vannucchi, P., 2004. Controls on tectonic accretion versus erosion in subduction zones: Implications for the origin and recycling of the continental crust. Rev. Geophys. 42 (2).
Cortecci, G., Frizzo, P., 1993. Origin of siderite deposits from the Lombardy Valleys, northern Italy: a carbon, oxygen and strontium isotope study. Chem. Geol. 105 (4), 293–303.
Dahlgren, R.A., Ugolini, F., Casey, W.H., 1999. Field weathering rates of Mt. St. Helens tephra. Geochim. Cosmochim. Acta 63 (5), 587–598.
Dasch, E.J., 1969. Strontium isotopes in weathering profiles, deep-sea sediments, and sedimentary rocks. Geochim. Cosmochim. Acta 33 (12), 1521–1552.
Declercq, J., Diedrich, T., Perrot, M., Gislason, S.R., Oelkers, E.H., 2013. Exp. erimental determination of rhyolitic glass dissolution rates at 40-200 degrees C and 2 < pH < 10.1. Geochim. Cosmochim. Acta 100, 251–263.
Elderfield, H., 1986. Strontium isotope stratigraphy. Palaeogeogr. Palaeoclimatol. Palaeoecol. 57 (1), 71–90.
Elderfield, H., Gieskes, J.M., 1982. Sr isotopes in interstitial waters of marine sediments from Deep Sea Drilling Project cores. Nature 300 (5892), 493.
Expedition 333 Scientists, 2012. In: Henry, P., Kanamatsu, T., Moe, K., E. Scientists (Eds.), Site C0012. Proceeding of the Integrated Ocean Drilling Program. Integrated Ocean Drilling Program Management International, Inc, Tokyo, pp. 333.
Expedition 337 Scientists, 2013a. In: Inagaki, F., Hinrichs, K.-U., Kubo, Y., t. E. Scientists (Eds.), Exp. Edition 337 Summary. Proceedings of the Integrated Ocean Drilling Program. Integrated Ocean Drilling Program Management International, Inc, Tokyo, pp. 337.
Expedition 337 Scientists, 2013b. In: Inagaki, F., Hinrichs, K.-U., Kubo, Y., t. E. Scientists (Eds.), Site C0020. Proceedings of the Integrated Ocean Drilling Program. Integrated Ocean Drilling Program Management International, Inc, Tokyo, pp. 337.
Fang, J., Kato, C., Runko, G., Nogi, Y., Hori, T., Li, J., Morono, Y., Inagaki, F., 2017. Predominance of viable spore-forming piezophilic bacteria in high-pressure enrichment cultures from ~1.5 to 2.4 km-deep coal-bearing sediments below the ocean floor. Front. Microbiol. 8 (137).
Faure, G., Powell, J.L., 1972. Strontium Isotope Geology. Springer, Berlin-Heidelberg-New York.
Fisk, M.R., Giovannoni, S.J., Thorseth, I.H., 1998. Alteration of oceanic volcanic glass: textural evidence of microbial activity. Science 281 (5379), 978–980.
Gerber, T.P., Pratson, L.F., Kuehl, S., Walsh, J., Alexander, C., Palmer, A., 2010. The influence of sea level and tectonics on Late Pleistocene through Holocene sediment storage along the high-sediment supply Waipaoa continental shelf. Mar. Geol. 270 (1–4), 139–159.
Gieskes, J.M., Lawrence, J.R., 1981. Alteration of volcanic matter in deep sea sediments: evidence from the chemical composition of interstitial waters from deep sea drilling cores. Geochim. Cosmochim. Acta 45 (10), 1687–1703.
Glombitza, C., Adhikari, R.R., Riedinger, N., Gilhooly, W.P., Hinrichs, K.-U., Inagaki, F., 2016. Microbial sulfate reduction potential in coal-bearing sediments down to ~2.5 km below the seafloor off Shimokita Peninsula, Japan. Front. Microbiol. 7 (1576).
Gross, D., Bechtel, A., Harrington, G.J., 2015. Variability in coal facies as reflected by organic petrological and geochemical data in Cenozoic coal beds offshore Shimokita (Japan)-IODP Exp. 337. Int. J. Coal Geol. 152, 63–79.
Harris, R., Sakaguchi, A., Petronotis, K., Baxter, A., Berg, R., Burkett, A., Charpentier, D., Choi, J., Ferreiro, P.D., Hamahashi, M., et al., 2013a. Expedition 344 summary. In: Harris, R.N., Sakaguchi, A., Petronotis, K., Expedition 344 Scientists (Eds.), Proc. IODP, 344. College Station, TX (Integrated Ocean Drilling Program). https://doi.org/10.2204/iodp.proc.344.101.2013.
Harris, R., Sakaguchi, A., Petronotis, K., Baxter, A., Berg, R., Burkett, A., Charpentier, D., Choi, J., Ferreiro, P.D., Hamahashi, M., et al., 2013b. Upper slope Site U1413. Proc. IODP, 344. College Station, TX (Integrated Ocean Drilling Program)https://doi.org/10.2204/iodp.proc.344.107.2013.
Heier, K., Compston, W., 1969. Rb− Sr isotopic studies of the plutonic rocks of the Oslo region. Lithos 2 (2), 133–145.
Henri, P.A., Rommevaux-Jestin, C., Lesongeur, F., Mumford, A., Emerson, D., Godfroy, A., Ménez, B., 2016. Structural iron (II) of basaltic glass as an energy source for zeta-proteobacteria in an abyssal plain environment, off the Mid Atlantic Ridge. Front. Microbiol. 6 (1518).
Henry, P., Kanamatsu, T., Moe, K.T., Strasser, M., 2012. IODP expedition 333: return to Nankai Trough subduction inputs sites and coring of mass transport deposits. Sci. Drill. 14, 4–17.
Hoefs, J., 2009. Stable Isotope Geochemistry. Springer.
Homoky, W., Hembury, D., Hepburn, L., Mills, R., Statham, P., Fones, G., Palmer, M., 2011. Iron and manganese diagenesis in deep sea volcanogenic sediments and the origins of pore water colloids. Geochim. Cosmochim. Acta 75 (17), 5032–5048.
von Huene, R., Scholl, D.W., 1991. Observation at convergent margins concerning sediment subduction, subduction erosion, and the growth of continental crust. Rev. Geophys. 29, 279–316.
Huhn, K., 2016. DSRV Sonne SO247 Cruise Report—SlamZ: Slide Activity on the Hikurangi Margin, New Zealand, Wellington–Auckland, 27 March–27 April 2016. Bundesministerium für Bildung und Forschung.
Inagaki, F., Hinrichs, K.-U., Kubo, Y., Bowles, M.W., Heuer, V.B., Hong, W.-L., Hoshino, T., Ijiri, A., Imachi, H., Ito, M., Kaneko, M., Lever, M.A., Lin, Y.-S., Methé, B.A., Morita, S., Morono, Y., Tanikawa, W., Bihan, M., Bowden, S.A., Elvert, M., Glombitza, C., Gross, D., Harrington, G.J., Hori, T., Li, K., Limmer, D., Liu, C.-H., Murayama, M., Ohkouchi, N., Ono, S., Park, Y.-S., Phillips, S.C., Prieto-Mollar, X., Purkey, M., Riedinger, N., Sanada, Y., Sauvage, J., Snyder, G., Susilawati, R., Takano, Y., Tasumi, E., Terada, T., Tomaru, H., Trembath-Reichert, E., Wang, D.T., Yamada, Y., 2015. Exp. Loring deep microbial life in coal-bearing sediment down to ~2.5 km below the ocean floor. Science 349 (6246), 420–424.
Jeans, C.V., Wray, D.S., Merriman, R.J., Fisher, M.J., 2000. Volcanogenic clays in Jurassic and Cretaceous strata of England and the North Sea basin. Clay Miner. 35 (1), 25–55.
Jørgensen, B.B., Boetius, A., 2007. Feast and famine—microbial life in the deep-sea bed. Nat. Rev. Microbiol. 5 (10), 770.
Joseph, C., Torres, M.E., Martin, R.A., Haley, B.A., Pohlman, J.W., Riedel, M., Rose, K., 2012. Using the 87Sr/86Sr of modern and paleoseep carbonates from northern Cascadia to link modern fluid flow to the past. Chem. Geol. 334 (0), 122–130.
Joseph, C., Torres, M.E., Haley, B., 2013a. Data report: 87Sr/86Sr in pore fluids from NanTroSEIZE Exp. editions 322 and 333. In: Saito, S., Underwood, M.B., Kubo, Y., the Exp. edition 322 Scientists (Eds.), Proceedings of the Integrated Ocean Drilling Program, pp. 322 Tokyo.
Joseph, C., Campbell, K.A., Torres, M.E., Martin, R.A., Pohlman, J.W., Riedel, M., Rose, K., 2013b. Methane-derived authigenic carbonates from modern and paleoseeps on the Cascadia margin: Mechanisms of formation and diagenetic signals. Palaeogeogr. Palaeoclimatol. Palaeoecol. 390, 52–67.
Kastner, M., 1981. Authigenic silicates in deep-sea sediments: formation and diagenesis. The sea 7, 915–980.
Kawai, M., Futagami, T., Toyoda, A., Takaki, Y., Nishi, S., Hori, S., Arai, W., Tsubouchi, T., Morono, Y., Uchiyama, I., Itoh, T., Fujiyama, A., Inagaki, F., Takami, H., 2014. High frequency of phylogenetically diverse reductive dehalogenase-homologous genes in deep subseafloor sedimentary metagenomes. Front. Microbiol. 5, 80.
Kennett, J.P., McBirney, A.R., Thunell, R.C., 1977. Episodes of Cenozoic volcanism in circum-Pacific region. J. Volcanol. Geotherm. Res. 2 (2), 145–163.
Kim, J.-H., Torres, M.E., Hong, W.-L., Choi, J., Riedel, M., Bahk, J.-J., Kim, S.-H., 2013. Pore fluid chemistry from the Second Gas Hydrate Drilling Exp. edition in the Ulleung Basin (UBGH2): source, mechanisms and consequences of fluid freshening in the central part of the Ulleung Basin, East Sea. Mar. Pet. Geol. 47, 99–112.
Kim, J.H., Torres, M.E., Haley, B.A., Ryu, J.S., Park, M.H., Hong, W.L., Choi, J., 2016. Marine silicate weathering in the anoxic sediment of the Ulleung Basin: evidence and consequences. Geochem. Geophys. Geosyst. 17 (8), 3437–3453.
Kutterolf, S., Freundt, A., Perez, W., Mörz, T., Schacht, U., Wehrmann, H., Schmincke, H.-U., 2008a. Pacific offshore record of plinian arc volcanism in Central America: 1. Along-arc correlations. Geochem. Geophys. Geosyst. 9 (2).
Kutterolf, S., Freundt, A., Peréz, W., 2008b. Pacific offshore record of plinian arc volcanism in Central America: 2. Tephra volumes and erupted masses. Geochem. Geophys. Geosyst. 9 (2).
Kutterolf, S., Schindlbeck, J.C., Scudder, R.P., Murray, R.W., Pickering, K.T., Freundt, A., Labanieh, S., Heydolph, K., Saito, S., Naruse, H., Underwood, M.B., Wu, H., 2014. Large volume submarine ignimbrites in the Shikoku Basin: an example for explosive volcanism in the Western Pacific during the late Miocene. Geochem. Geophys. Geosyst. 15, 1837–1851. https://doi.org/10.1002/2014GC005263.
Kutterolf, S., Schindlbeck, J., Robertson, A., Avery, A., Baxter, A., Petronotis, K., Wang, K.L., 2018. Tephrostratigraphy and provenance from IODP Exp. edition 352, Izu-Bonin arc: Tracing tephra sources and volumes from the Oligocene to recent. Geochem. Geophys. Geosyst. 19 (1), 150–174.
Kuznetsov, A., Krupenin, M., Ovchinnikova, G., Gorokhov, I., Maslov, A., Kaurova, O., Ellmies, R., 2005. Diagenesis of carbonate and siderite deposits of the Lower Riphean Bakal Formation, the Southern Urals: Sr isotopic characteristics and Pb-Pb age. Lithol. Miner. Resour. 40 (3), 195–215.
Lawrence, J.R., Drever, J.I., Anderson, T.F., Brueckner, H.K., 1979. Importance of alteration of volcanic material in the sediments of deep sea drilling site 323: chemistry, 18O16O and 87Sr86Sr. Geochim. Cosmochim. Acta 43 (4), 573–588.
Ledbetter, M.T., Sparks, R.S.J., 1979. Duration of large-magnitude explosive eruptions deduced from graded bedding in deep-sea ash layers. Geology 7 (5), 240–244.
Lewis, K.B., Lallemand, S.E., Carter, L., 2004. Collapse in a Quaternary shelf basin off East Cape, New Zealand: evidence for passage of a subducted seamount inboard of the Ruatoria giant avalanche. N. Z. J. Geol. Geophys. 47 (3), 415–429.
Longman, J., Palmer, M.R., Gernon, T.M., Manners, H.R., 2019. The role of tephra in enhancing organic carbon preservation in marine sediments. Earth Sci. Rev. 192, 480–490.
Luo, M., Torres, M.E., Hong, W.-L., Pape, T., Fronzek, J., Kutterolf, S., Mountjoy, J.J., Orpin, A., Henkel, S., Huhn, K., Chen, D., Kasten, S., 2020. Impact of iron release by volcanic ash alteration on carbon cycling in sediments of the northern Hikurangi margin. Earth Planet. Sci. Lett. 541, 116288.
Mahony, S., Wallace, L., Miyoshi, M., Villamor, P., Sparks, R., Hasenaka, T., 2011. Volcano-tectonic interactions during rapid plate-boundary evolution in the Kyushu region, SW Japan. Bulletin 123 (11−12), 2201–2223.
Mayer, L.M., 1994. Relationships between mineral surfaces and organic carbon concentrations in soils and sediments. Chem. Geol. 114 (3–4), 347–363.
Moen, N., Hong, W.-L., Haley, B., 2015. Data report: 87Sr/86Sr in pore fluids off Shimokita, Japan. In: Proc. IODP| Volume **337**, pp. 2.

Mork, M.B.E., Leith, D.A., Fanavoll, S., 2001. Origin of carbonate-cemented beds on the Naglfar Dome, Voring Basin, Norwegian Sea. Mar. Pet. Geol. 18 (2), 223–234.
Orpin, A., 2004. Holocene sediment deposition on the Poverty-slope margin by the muddy Waipaoa River, East Coast New Zealand. Mar. Geol. 209 (1–4), 69–90.
Orpin, A.R., Alexander, C., Carter, L., Kuehl, S., Walsh, J., 2006. Temporal and spatial complexity in post-glacial sedimentation on the tectonically active, Poverty Bay continental margin of New Zealand. Cont. Shelf Res. 26 (17–18), 2205–2224.
Palmer, M., Edmond, J., 1989. The strontium isotope budget of the modern ocean. Earth Planet. Sci. Lett. 92 (1), 11–26.
Paquet, F., Proust, J.-N., Pettinga, J., Barnes, P., 2006. The pleistocene forearc basin of the Hikurangi subduction, Eastern North island, New Zealand: Erosion, sedimentation and tectonic evolution. In: Geophysical Research Abstracts, European Geosciences Union General Assembly 2006.
Paquet, F., Proust, J.-N., Barnes, P.M., Pettinga, J.R., 2011. Controls on active forearc basin stratigraphy and sediment fluxes: the Pleistocene of Hawke Bay, New Zealand. Bulletin 123 (5–6), 1074–1096.
Parruzot, B., Jollivet, P., Rébiscoul, D., Gin, S., 2015. Long-term alteration of basaltic glass: mechanisms and rates. Geochim. Cosmochim. Acta 154, 28–48.
Pearce, C.R., Parkinson, I.J., Gaillardet, J., Charlier, B.L., Mokadem, F., Burton, K.W., 2015. Reassessing the stable (δ88/86Sr) and radiogenic (87Sr/86Sr) strontium isotopic composition of marine inputs. Geochim. Cosmochim. Acta 157, 125–146.
Phillips, M.P., Harwood, D.M., Harrington, G.J., 2016. Neogene and early Pleistocene diatom biostratigraphy and age synthesis of Site C9001/C0020, Northwest Pacific. Mar. Micropaleontol. 128, 39–49.
Phillips, S.C., Johnson, J.E., Clyde, W.C., Setera, J.B., Maxbauer, D.P., Severmann, S., Riedinger, N., 2017. Rock magnetic and geochemical evidence for authigenic magnetite formation via iron reduction in coal-bearing sediments offshore Shimokita Peninsula, Japan (IODP Site C0020). Geochem. Geophys. Geosyst. 18 (6), 2076–2098.
Phillips, S.C., Hong, W.-L., Johnson, J.E., Fahnestock, M.F., Bryce, J.G., 2018. Authigenic carbonate formation influenced by freshwater inputs and methanogenesis in coal-bearing strata offshore Shimokita, Japan (IODP site C0020). Mar. Pet. Geol. 96, 288–303.
Plank, T., Langmuir, C.H., 1998. The chemical composition of subducting sediment and its consequences for the crust and mantle. Chem. Geol. 145 (3–4), 325–394.
Pouderoux, H., Proust, J.-N., Lamarche, G., Orpin, A., Neil, H., 2012. Postglacial (after 18 ka) deep-sea sedimentation along the Hikurangi subduction margin (New Zealand): Characterisation, timing and origin of turbidites. Mar. Geol. 295, 51–76.
Ranero, C.R., von Huene, R., 2000. Subduction erosion along the Middle America convergent margin. Nature 404 (6779), 748.
Ranero, C., Von Huene, R., Flueh, E.R., Weinrebe, W., Hinz, K., Leandro, G., Alvarado, G., Duarte, M., 2000. Lower plate control on subduction erosion processes along the middle America convergent margin. Z. Angew. Geol. 291–296.
Rogers, J.R., Bennett, P.C., 2004. Mineral stimulation of subsurface microorganisms: release of limiting nutrients from silicates. Chem. Geol. 203 (1–2), 91–108.
Rose, K.K., Johnson, J.E., Torres, M.E., Hong, W., Giosan, L., Solomon, E.A., Kastner, M., Cawthern, T., Long, P.E., Schaef, H.T., 2014. Anomalous porosity preservation and preferential accumulation of gas hydrate in the Andaman Accretionary Wedge, NGHP-01 Site 17A. Mar. Pet. Geol. 58, 99–116.
Ross, N., Torres, M.E., Haley, B.A., Solomon, E.A., Kastner, M., 2015. Data report: Strontium isotope analyses of pore fluids from the CRISP-A transect drilled during Exp. editions 334 and 344. In: Proc. IODP| Volume.
Roy, M., McManus, J., Goni, M.A., Chase, Z., Borgeld, J.C., Wheatcroft, R.A., Muratli, J.M., Megowan, M.R., Mix, A., 2013. Reactive iron and manganese distributions in seabed sediments near small mountainous rivers off Oregon and California (USA). Cont. Shelf Res. 54, 67–79.
Saito, S., Underwood, M.B., Kubo, Y., E. Scientists, 2010. Proc. IODP. Integrated Ocean Drilling Program Management International, Inc., Tokyo, pp. 322.
Sample, J.C., Torres, M.E., Fisher, A., Hong, W.-L., Destrigneville, C., Defliese, W.F., Tripati, A.E., 2017. Geochemical constraints on the temperature and timing of carbonate formation and lithification in the Nankai Trough, NanTroSEIZE transect. Geochim. Cosmochim. Acta 198, 92–114.
Schacht, U., 2005. Alteration of Volcanic Glasses in Marine Sediments: Laboratory Experiments and Field Studies. Christian-Albrechts Universität Kiel.
Schindlbeck, J.C., Kutterolf, S., Freundt, A., Alvarado, G., Wang, K.L., Straub, S., Hemming, S., Frische, M., Woodhead, J., 2016a. Late Cenozoic tephrostratigraphy offshore the southern Central American Volcanic Arc: 1. Tephra ages and provenance. Geochem. Geophys. Geosyst. 17 (11), 4641–4668.
Schindlbeck, J.C., Kutterolf, S., Freundt, A., Straub, S., Vannucchi, P., Alvarado, G., 2016b. Late Cenozoic tephrostratigraphy offshore the southern Central American Volcanic Arc: 2. Implications for magma production rates and subduction erosion. Geochem. Geophys. Geosyst. 17 (11), 4585–4604.
Scudder, R.P., Murray, R.W., Plank, T., 2009. Dispersed ash in deeply buried sediment from the northwest Pacific Ocean: an example from the Izu-Bonin arc (ODP Site 1149). Earth Planet. Sci. Lett. 284 (3–4), 639–648.
Scudder, R.P., Murray, R.W., Schindlbeck, J.C., Kutterolf, S., Hauff, F., Underwood, M.B., Gwizd, S., Lauzon, R., McKinley, C.C., 2016. Geochemical approaches to the quantification of dispersed volcanic ash in marine sediment. Prog. Earth Planet. Sci. 3 (1), 1.
Scudder, R.P., Murray, R.W., Kutterolf, S., Schindlbeck, J.C., Underwood, M.B., Wang, K.-L., 2018. Sedimentary inputs to the Nankai subduction zone: the importance of dispersed ash. Geosphere. https://doi.org/10.1130/GES01558.1.
Seyfried Jr., W., Bischoff, J., 1979. Low temperature basalt alteration by sea water: an experimental study at 70 C and 150 C. Geochim. Cosmochim. Acta 43 (12), 1937–1947.
Shikazono, N., Takino, A., Ohtani, H., 2005. An estimate of dissolution rate constant of volcanic glass in volcanic ash soil from the Mt. Fuji area, central Japan. Geochem. J. 39 (2), 185–196.
Solomon, E.A., Spivack, A.J., Kastner, M., Torres, M.E., Robertson, G., 2014. Gas hydrate distribution and carbon sequestration through coupled microbial methanogenesis and silicate weathering in the Krishna–Godavari Basin, offshore India. Mar. Pet. Geol. 58 (Part A), 233–253.
Spinelli, G.A., Hutton, A., 2013. Data report: Amorphous silica content of sediment from Sites C0011 and C0012 in the Shikoku Basin on the NanTroSEIZE transect. In: Saito, S., Underwood, M.B., Kubo, Y., E. Scientists (Eds.), Proceeding of the Integrated Ocean Drilling Program. Integrated Ocean Drilling Program Management International, Inc, Tokyo, pp. 322.
Spinelli, G.A., Mozley, P.S., Tobin, H.J., Underwood, M.B., Hoffman, N.W., Bellew, G.M., 2007. Diagenesis, sediment strength, and pore collapse in sediment approaching the Nankai Trough subduction zone. Geol. Soc. Am. Bull. 119 (3–4), 377–390.
Steuber, T., Veizer, J.n., 2002. Phanerozoic record of plate tectonic control of seawater chemistry and carbonate sedimentation. Geology 30 (12), 1123–1126.
Stonestrom, D.A., White, A.F., Akstin, K.C., 1998. Determining rates of chemical weathering in soils—Solute transport versus profile evolution. J. Hydrol. 209 (1–4), 331–345.
Stranghoener, M., Schippers, A., Dultz, S., Behrens, H., 2018. Exp. erimental Microbial Alteration and Fe Mobilization from Basaltic Rocks of the ICDP HSDP2 Drill Core, Hilo, Hawaii. Front. Microbiol. 9 (1252).
Sutton, A.N., Blake, S., Wilson, C.J., 1995. An outline geochemistry of rhyolite eruptions from Taupo volcanic centre, New Zealand. J. Volcanol. Geotherm. Res. 68 (1–3), 153–175.
Taylor, A.S., Blum, J.D., Lasaga, A.C., MacInnis, I.N., 2000. Kinetics of dissolution and Sr release during biotite and phlogopite weathering. Geochim. Cosmochim. Acta 64 (7), 1191–1208.
Tomaru, H., Fehn, U., Lu, Z., Takeuchi, R., Inagaki, F., Imachi, H., Kotani, R., Matsumoto, R., Aoike, K., 2009. Dating of dissolved iodine in pore waters from the gas hydrate occurrence offshore Shimokita Peninsula, Japan: 129I results from the D/V Chikyu shakedown cruise. Resour. Geol. 59 (4), 359–373.
Torres, M., Cox, T., Hong, W.L., McManus, J., Sample, J., Destrigneville, C., Gan, H., Gan, H., Moreau, J., 2015. Crustal fluid and ash alteration impacts on the biosphere of Shikoku Basin sediments, Nankai Trough, Japan. Geobiology 13 (6), 562–580.
Torres, M.E., Hong, W.-L., Solomon, E.A., Milliken, K., Kim, J.-H., Sample, J., Teichert, B., Wallmann, K., 2020. Review of silicate weathering in anoxic marine sediment and its role in authigenic carbonate burial. Earth Sci. Rev. 200, 102960.
Trembath-Reichert, E., Morono, Y., Ijiri, A., Hoshino, T., Dawson, K.S., Inagaki, F., Orphan, V.J., 2017. Methyl-compound use and slow growth characterize microbial life in 2-km-deep subseafloor coal and shale beds. Proc. Natl. Acad. Sci. 114 (44), E9206–E9215.
Underwood, M.B., Moore, G.F., Taira, A., Klaus, A., Wilson, M.E., Fergusson, C.L., Hirano, S., Steurer, J., 2003. Sedimentary and tectonic evolution of a trench-slope basin in the Nankai subduction zone of southwest Japan. J. Sediment. Res. 73 (4), 589–602.
Underwood, M.B., Saito, S., Kubo, Y., E. Scientists, 2010. In: Saito, S., Underwood, M.B., Kubo, Y., E. Scientists (Eds.), Exp. Edition 322 Summary. Proceeding of the Integrated Ocean Drilling Program. Integrated Ocean Drilling Program Management International, Inc, Tokyo, pp. 322.
Valle, N., Verney-Carron, A., Sterpenich, J., Libourel, G., Deloule, E., Jollivet, P., 2010. Elemental and isotopic (Si-29 and O-18) tracing of glass alteration mechanisms. Geochim. Cosmochim. Acta 74 (12), 3412–3431.
Vannucchi, P., Galeotti, S., Clift, P.D., Ranero, C.s.R., von Huene, R., 2004. Long-term subduction-erosion along the Guatemalan margin of the Middle America Trench. Geology 32 (7), 617–620.
Veizer, J., 1989. Strontium isotopes in seawater through time. Annu. Rev. Earth Planet. Sci. 17, 141–167.
Vollstaedt, H., Eisenhauer, A., Wallmann, K., Böhm, F., Fietzke, J., Liebetrau, V., Krabbenhöft, A., Farkaš, J., Tomašových, A., Raddatz, J., 2014. The Phanerozoic δ88/86Sr record of seawater: New constraints on past changes in oceanic carbonate fluxes. Geochim. Cosmochim. Acta 128, 249–265.
Wallmann, K., Aloisi, G., Haeckel, M., Tishchenko, P., Pavlova, G., Greinert, J., Kutterolf, S., Eisenhauer, A., 2008. Silicate weathering in anoxic marine sediments. Geochim. Cosmochim. Acta 72 (12), 2895–2918.
White, A.F., Bullen, T.D., Schulz, M.S., Blum, A.E., Huntington, T.G., Peters, N.E., 2001. Differential rates of feldspar weathering in granitic regoliths. Geochim. Cosmochim. Acta 65 (6), 847–869.
White, R.J., Spinelli, G.A., Mozley, P.S., Dunbar, N.W., 2011. Importance of volcanic glass alteration to sediment stabilization: offshore Japan. Sedimentology 58 (5), 1138–1154.
Wilson, C., Blake, S., Charlier, B., Sutton, A., 2006. The 26.5 ka Oruanui eruption, Taupo volcano, New Zealand: development, characteristics and evacuation of a large rhyolitic magma body. J. Petrol. 47 (1), 35–69.
Wolff-Boenisch, D., Gislason, S.R., Oelkers, E.H., Putnis, C.V., 2004. The dissolution rates of natural glasses as a function of their composition at pH 4 and 10.6, and temperatures from 25 to 74 C. Geochim. Cosmochim. Acta 68 (23), 4843–4858.
Yokoyama, T., 2013. Characterization of the reaction and transport properties of porous rhyolite and its application to the quantitative understanding of the chemical weathering rate. Geochim. Cosmochim. Acta 118, 295–311.
Yokoyama, T., Banfield, J.F., 2002. Direct determinations of the rates of rhyolite dissolution and clay formation over 52,000 years and comparison with laboratory measurements. Geochim. Cosmochim. Acta 66 (15), 2665–2681.